Is the sky falling? Searching for stellar streams in the local Milky Way disc in the CORAVEL and RAVE surveys

G. M. Seabroke[1]*, G. Gilmore[1], A. Siebert[2], O. Bienaymé[3], J. Binney[4],
J. Bland-Hawthorn[5], R. Campbell[6], K. C. Freeman[7], B. Gibson[8],
E. K. Grebel[9,10], A. Helmi[11], U. Munari[12], J. F. Navarro[13], Q. A. Parker[6,5],
A. Siviero[12], M. Steinmetz[2], F. G. Watson[5], R. F. G. Wyse[14], T. Zwitter[15],
J. Peñarrubia[13], M. C. Smith[1], M. Williams[7]

[1] *Institute of Astronomy, University of Cambridge, Madingley Road, Cambridge, CB3 0HA, UK*
[2] *Astrophysikalisches Institut Potsdam, An der Sterwarte 16, D-14482 Potsdam, Germany*
[3] *Observatoire de Strasbourg, 11 Rue de L'Université, 67000 Strasbourg, France*
[4] *Rudolf Peierls Centre for Theoretical Physics, University of Oxford, 1 Keble Road, Oxford OX1 3NP, UK*
[5] *Anglo-Australian Observatory, P.O. Box 296, Epping, NSW 1710, Australia*
[6] *Macquarie University, Sydney, NSW 2109, Australia*
[7] *RSAA, Mount Stromlo Observatory, Cotter Road, Weston Creek, Canberra, ACT 72611, Australia.*
[8] *University of Central Lancashire, Preston PR1 2HE, UK*
[9] *Astronomisches Institut, Universität Basel, Venusstrasse 7, Binningen CH-4102, Switzerland*
[10] *Astronomisches Rechen-Institut, Zentrum für Astronomie der Universität Heidelberg, Mönchhofstr. 12-14, D-69120 Heidelberg, Germany*
[11] *Kapteyn Astronomical Institute, University of Groningen, P.O. Box 800, 9700 AV Groningen, The Netherlands*
[12] *INAF Osservatorio Astronomico di Padova, Via dell'Osservatorio 8, Asiago I-36012, Italy*
[13] *University of Victoria, P.O. Box 3055, Station CSC, Victoria, BC V8W 3P6, Canada*
[14] *Johns Hopkins University, 366 Bloomberg Center, 3400 North Charles Street, Baltimore, MD 21218, USA*
[15] *Department of Physics, University of Ljubljana, Jadranska 19, Ljubljana, Slovenia*

ABSTRACT

We have searched for in-falling stellar streams on to the local Milky Way disc in the CORAVEL and RAVE surveys. The CORAVEL survey consists of local dwarf stars (Nördstrom et al. Geneva-Copenhagen survey) and local Famaey et al. giant stars. We select RAVE stars with radial velocities that are sensitive to the Galactic vertical space velocity (Galactic latitude $b < -45°$). Kuiper statistics have been employed to test the symmetry of the Galactic vertical velocity distribution functions in these samples for evidence of a net vertical flow that could be associated with a (tidal?) stream of stars with vertically coherent kinematics. In contrast to the 'Field of Streams' found in the outer halo, we find that the local volumes of the solar neighbourhood sampled by the CORAVEL dwarfs (complete within $\sim 3 \times 10^{-4}$ kpc^3), CORAVEL giants (complete within $\sim 5 \times 10^{-2}$ kpc^3) and RAVE (5-15 per cent complete within ~ 8 kpc^3) are devoid of any vertically coherent streams containing hundreds of stars. This is sufficiently sensitive to allow our RAVE sample to rule out the passing of the tidal stream of the disrupting Sagittarius (Sgr) dwarf galaxy through the solar neighbourhood. This agrees with the most recent determination of its orbit and dissociates it from the Helmi et al. halo stream. Our constraints on the absence of the Sgr stream near the Sun could prove a useful tool for discriminating between Galactic potential models. The lack of a net vertical flow through the solar neighbourhood in the CORAVEL giants and RAVE samples argues against the Virgo overdensity crossing the disc near the Sun. There are no vertical streams in the CORAVEL giants and RAVE samples with stellar densities $\gtrsim 1.6 \times 10^4$ and 1.5×10^3 stars kpc^{-3} respectively and therefore no evidence for locally enhanced dark matter.

Key words: solar neighbourhood; Galaxy: disc; Galaxy: formation; Galaxy: kinematics and dynamics; Galaxy: structure; dark matter

1   INTRODUCTION

Tidal streams are filaments of debris, containing stars, gas and possibly dark matter (DM), that have become stripped from a disrupting satellite dwarf galaxy (or star cluster) along its orbit with respect to the centre-of-mass of a more massive galaxy. The instantaneous position and velocity of a star and the Galactic gravitational potential determines its past orbit. For stars in tidal streams, one can most reliably know their positions and velocities in the past. This is because stars in tidal streams all originate, at one time in the past, from a single progenitor on a specific orbit. It is this property of tidal streams that makes them excellent tracers of the Galactic potential (Johnston et al. 1999; Murali & Dubinski 1999) while the degree of tidal-stream coherence provides a powerful constraint on the lumpiness of the Galactic potential (Johnston et al. 2002).

The disruption timescales of merging galaxies (Helmi & White 1999, hereafter H99a) means the discovery of new tidal streams, e.g. the Orphan stream (Belokurov et al. 2006, 2007; Grillmair 2006), can also lead to the discovery of new satellites, e.g. Ursa Major II (UMa II, Zucker et al. 2006; Fellhauer et al. 2007a), which are of relevance to the 'missing satellite problem' (Moore et al. 1999; Klypin et al. 1999; Benson et al. 2002). These discoveries offer more evidence of the hierarchical structure formation of the Milky Way Galaxy and provide accretion history constraints for simulations of this process (e.g. Abadi et al. 2003). If a tidal stream containing DM is passing through the solar neighbourhood, it would provide a 'cold' flow of DM particles through the numerous direct detection experiments on Earth, increasing the possibility of a positive direct detection (Freese et al. 2004).

The first evidence that there may be tidal streams in the solar neighbourhood was the discovery of two streams (Helmi et al. 1999, hereafter H99b) in kinematic surveys of the local stellar halo (Beers & Sommer-Larsen 1995; Chiba & Yoshii 1998). This discovery was subsequently confirmed by Chiba & Beers (2000) and Kepley et al. (2007).

The most spectacular example of tidal streams is from the disruption of the Sagittarius (Sgr) dwarf spheroidal (dSph) galaxy, originally discovered by Ibata et al. (1994). Estimates of the central mass-to-light ratios of dwarf galaxies are high, suggesting they and plausibly their tidal streams are all DM-dominated. The most extensive sky panorama of the Sgr stream is traced by M giants (Majewski et al. 2003) from the Two-Micron All-Sky Survey (2MASS). The stream is seen very clearly in the Southern Galactic hemisphere, as well as heading towards the North Galactic Pole (NGP). Majewski et al. (2003) found the stream lies along a well-defined orbital plane about the Galactic centre and speculated that the foreshortening of the stream towards the NGP means it heads back towards the Galactic plane. The Sun lies within ~ 1 kpc of that plane, which is within the width of the stream, leading Majewski et al. (2003) to propose the possibility that the stream crosses the Galactic plane near or in the solar neighbourhood. Freese et al. (2004) postulated that one of the H99b streams is part of the Sgr stream passing through the solar neighbourhood and that its DM density should be measurable in direct detection experiments.

Law et al. (2005) modelled the Sgr stream and found that its two arms pass through a similar position in the plane of the sky, near the Virgo overdensity (VOD). Martínez-Delgado et al. (2007) suggest that the VOD is part of the Sgr stream, which crosses the Milky Way plane in the solar neighbourhood, and show that the Law et al. (2005) model passes through the observed location of the VOD and the VOD stellar density is similar to the model predictions. However, there is a growing weight of evidence against the Sgr stream existing in the solar neighbourhood. Dynamical analyses of the multiple wraps of the Sgr stream and the newly discovered Orphan stream found in the 'Field of Streams' (Belokurov et al. 2006) suggest that neither the Sgr (Fellhauer et al. 2006) nor Orphan streams (Fellhauer et al. 2007b) pass near the Sun. More recently, (Newberg et al. 2007) used Sloan Digital Sky Survey (SDSS) imaging and Sloan Extension for Galactic Understanding and Exploration (SEGUE) spectroscopic observations of F turnoff and blue horizontal branch (BHB) stars to show that the Sgr stream is neither coincident with the VOD nor passes through the solar neighbourhood. Instead, they find that it misses the Sun by 15 kpc, passing through the plane well outside the solar circle.

Juric et al. (2005) used SDSS photometry to identify the VOD – the largest clump of tidal debris so far detected in the outer halo. It covers ~ 1000 deg^2 above the Galactic plane ($5 < Z < 15$ kpc), over the solar position in the Galaxy ($R \sim 7$ kpc). They interpreted it as a tidal stream or an invading dwarf galaxy. Juric et al. (2005) did not detect any downturn in the star counts towards lower Galactic latitudes (b), indicating the VOD could extend closer to the Galactic plane than the observations probe ($b > 60°$).

With the advent of SDSS Data Release 5 and the discoveries of the VOD and Orphan stream, Fuchs et al. (2006) re-analysed star counts from their Calar Alto Deep Imaging Survey (CADIS) data. In retrospect, they find that overdensities in the vertical-density distribution of stars can be associated with the VOD in the 13-h CADIS field and possibly the Monoceros (Newberg et al. 2002) and Orphan streams in the 9-h CADIS field. Simulations by Fellhauer et al. (2007a) show the 9-h field falls on the second wrap of the backward orbit of UMa II before it passes along the Orphan stream. In this direction, Fellhauer et al. (2007a) demonstrated that the Orphan stream is >30 kpc from the Sun and its orbit does not bring it much closer to the solar neighbourhood (see their fig. 2).

The Monoceros stream is seen in the data of Juric et al. (2005) at $3 \lesssim Z \lesssim 5$ kpc and $R \sim 16$ kpc. Two other overdensities are also visible in the top right plot of Juric et al. (2005) fig. 20 at $(R, Z) \sim (1.5, 6.5)$ and $(9, 0.8)$ kpc (the latter is seen most clearly in the second row, right plot). None of these four overdensities are seen to exist in the solar neighbourhood. Peñarrubia et al. (2005) have modelled the Monoceros stream and their simulations show that part of it may be seen in the direction of the 9-h field at heliocentric distances of the overdensity in the 9-h field (3-21 kpc), again far from the solar neighbourhood.

Unlike in the Galactic disc, tidal streams in the outer halo are not phase-mixed quickly due to its dynamical timescale of >1 Gyr and so remain coherent in configuration space for longer than in the disc. The low stellar density in the outer halo enables large tidal streams to be identified as stellar overdensities in photometric surveys like the SDSS.

The shorter dynamical timescales and much higher stellar densities cause tidal streams in the inner Galaxy to quickly lose their coherence in configuration space but they remain coherent in velocity space (H99a).

Until recently, the full six-dimensional phase space of the solar neighbourhood had not been systematically surveyed. This was because, although the *Hipparcos* satellite mission (ESA 1997) provided accurate parallaxes and proper motions for ∼118 000 stars, these stars generally lacked radial velocities (RVs). Therefore, a large European consortium obtained kinematically unbiased RVs of *Hipparcos* stars of spectral type later than about F5 (Udry et al. 1997). Multi-epoch RVs of ∼45 000 stars were measured with the two CORrelation RAdial VELocities (CORAVEL) photoelectric cross-correlation spectrometers (Baranne et al. 1979; Mayor 1985). There have been two public data releases and three published analyses of stars in the CORAVEL database: the Geneva-Copenhagen survey of 16 682 nearby CORAVEL F-G dwarfs, available via VizieR, is described and analysed in Nordström et al. (2004), hereafter N04, and recently re-analysed in Holmberg et al. (2007); and a catalogue of the local kinematics of 6691 CORAVEL K-M giants, also available via VizieR, is described and analysed by Famaey et al. (2005), hereafter F05.

The RAdial Velocity Experiment (RAVE, Steinmetz et al. 2006) is a spectroscopic survey measuring the RVs and stellar atmosphere parameters (temperature, metallicity and surface gravity) of up to one million stars in the range of magnitudes probing Galactic scales between the very local CORAVEL RV surveys and the more distant SEGUE RV survey. RAVE started in 2003, using the Six-Degree Field (6dF) multi-object spectrograph on the 1.2-m UK Schmidt Telescope of the Anglo-Australian Observatory in Australia.

The recent, timely availability of the CORAVEL and RAVE data sets permit direct searches for the presence of tidal streams in the solar neighbourhood. Helmi et al. (2006) have already searched the N04 CORAVEL dwarf data set for signatures of past accretion on to the local disc. They find that stars with a common progenitor should show distinct correlations between orbital apocentre (A), pericentre (P) and Z angular momentum (J_Z). In APJ-space, their analysis reveals a statistically significant excess of stars on orbits of common eccentricity, analogous to the pattern expected for merger debris. They identify three coherent groups with distinct metallicity and age distributions that they assert correspond to the remains of disrupted satellites.

In this paper, we (quite literally) take an orthogonal approach by simply posing the question: is there any net vertical flow through the solar neighbourhood? This is a different question to that explored by Gould (2003) and Bell et al. (2007): we are not attempting to constrain the amount of phase-space substructure. The well-established Galactic stellar components in the solar neighbourhood (thin and thick discs and inner halo) are kinematically symmetric about the Galactic plane. Therefore, any net vertical flow could reasonably be associated with a tidal stream of stars with vertically coherent kinematics. Hence, within the sample volumes of the CORAVEL and RAVE surveys, we can directly test whether the Sgr stream and VOD pass near the Sun and consequently whether direct DM detection experiments should expect enhanced modulated signals from these or any other streams.

We organize the paper by analysing the data sets in order of increasing sampled volume. Ergo, we begin with the CORAVEL dwarfs in Section 2. In Section 2.3, we use this sample to show that the effect of binarity is negligible in the analysis of velocity distribution functions, which is important for our purpose here as well as many future science applications of RAVE and SEGUE data. We introduce our statistical test to identify streams in Section 2.4. This test is applied to the CORAVEL giants in Section 3 and all the RAVE stars in Section 4.

This is not the first science paper to make use of the RAVE data set. Smith et al. (2007) used high-velocity RAVE stars to constrain the local Galactic escape speed. Veltz et al. (2007) used 2MASS to select RAVE stars with $0.5 \leqslant J - K_S \leqslant 0.7$, which corresponds to K3-K7 dwarfs and G3-K1 (red clump) giants, to identify kinematic and density discontinuities between the thin disc, thick disc and inner halo towards the South Galactic Pole (SGP). We introduce the RAVE stellar populations in Section 4.1. We discuss our results in Section 5 before ending on an historical aside in Appendix A.

2 CORAVEL DWARFS

2.1 Derivation of the space velocities of the CORAVEL dwarfs

The Geneva-Copenhagen survey is complete, all-sky, magnitude-limited and kinematically unbiased. Its observational input catalogue was selected from a compilation of catalogues available in the literature with Strömgren $uvby\beta$ photometry of nearby F and G stars, mainly from the surveys by Olsen (1983, 1993, 1994a,b). The input catalogue was observed using both CORAVELs. Their fixed, late-type cross-correlation template spectra match the spectra of the majority of the input catalogue stars. The multi-epoch RVs (generally two or more) have a modal mean error of the mean RVs of 0.25 km s^{-1} (see N04 fig. 3).

The vast majority of these stars have proper motions in the *Tycho-2* catalogue (Høg et al. 2000). This catalogue was constructed by combining the *Tycho* star-mapper measurements of the *Hipparcos* satellite with the Astrographic Catalogue based on measurements in the Carte du Ciel and other ground-based catalogues. The typical mean error in the total proper motion vector is 1.8 mas yr^{-1}.

The primary source of distance for these stars is *Hipparcos* trigonometric parallax. This is adopted if its relative error (σ_π/π) is accurate to 13 per cent or better, otherwise the photometric distance calibrations for F and G dwarfs by Crawford (1975) and Olsen (1984) are used, with an uncertainty of only 13 per cent. Distances are not provided for stars with unreliable *Hipparcos* parallax ($\sigma_\pi/\pi > 13$ per cent) and when photometric distances cannot be calculated. This occurs when the star is missing the necessary photometry and/or it falls outside the photometric calibrations. The absence of a distance estimate or RV measurement reduces the size of the sample with all full six dimensional phase-space information to 13 240 stars. The space velocity components in the Galactic cardinal directions, U (towards the
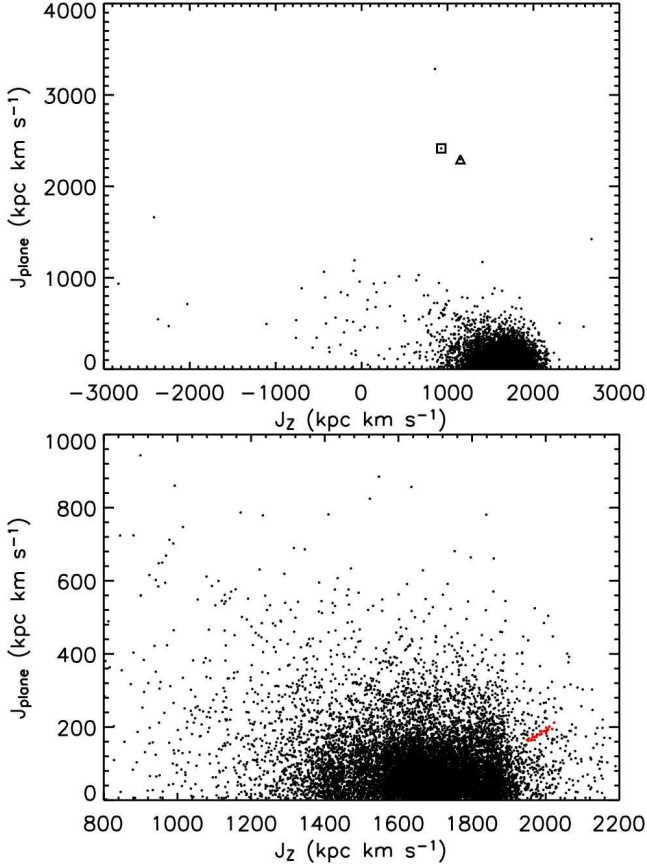
Figure 1. Distribution of CORAVEL dwarfs in the plane of orbital angular momentum components, where $J_{plane} = \sqrt{J_X^2 + J_Y^2}$. *Top*: The triangle is star HD 175305 and the square is CD -80 328. *Bottom*: The red dots are stars in an apparent linear structure.

Galactic centre), V (in the direction of Galactic rotation) and W (towards the NGP), are computed for all the stars with (mean) RVs, proper motions and distances.

2.2 Orbital angular momenta of the CORAVEL dwarfs

The availability of distances to each CORAVEL dwarf allows their Galactic-centred cartesian co-ordinates (X, Y, Z) to be calculated, where $(X_\odot, Y_\odot, Z_\odot) = (8, 0, 0)$ kpc, which in combination with their (U, V, W) relative to the Galactic Standard of Rest (GSR) permits their components of orbital angular momentum (J) to be resolved into

$$J_X = YW_{GSR} - ZV_{GSR}, \tag{1}$$
$$J_Y = ZU_{GSR} - XW_{GSR}, \tag{2}$$
$$J_Z = XV_{GSR} - YU_{GSR}, \tag{3}$$

where

$$U_{GSR} = U_{LSR} = U + U_{LSR}^\odot, \tag{4}$$
$$V_{GSR} = V_{LSR} + V_{rot} = V + V_{LSR}^\odot + V_{rot}, \tag{5}$$
$$W_{GSR} = W_{LSR} = W + W_{LSR}^\odot, \tag{6}$$

where $(U_{LSR}^\odot, V_{LSR}^\odot, W_{LSR}^\odot) = (10.00, 5.25, 7.17)$ km s^{-1} (Dehnen & Binney 1998) is the solar motion, decomposed into its cardinal directions, relative to the Local Standard of Rest (LSR), and $V_{rot} = 220$ km s^{-1} is the amplitude of Galactic rotation towards $l = 90°$ and $b = 0°$ (IAU 1985 convention; see Kerr & Lynden-Bell 1986). Fig. 1 shows the CORAVEL dwarf sample is dominated by high-angular momentum disc stars with only ~100 low-angular momentum halo stars.

Two stars on prograde high-inclination orbits (the triangle and square in the top plot of Fig. 1) share similar angular momenta as the H99b streams (cf. their fig. 2). The triangle in the top plot of Fig. 1 is HD 175305 and has a photometric metallicity of -1.39 dex. It is also in the Beers & Sommer-Larsen (1995) and Chiba & Yoshii (1998) catalogues with spectroscopic metallicities of -1.42 and -1.54 dex respectively. Its kinematics, $(U, V, W)_{GSR} = (-58, 142, -286)$ km s^{-1}, means it is one of the stars in the H99b stream moving towards the SGP. Beers et al. (2000) and Kepley et al. (2007) explicitly cite this star as a member of one of the H99b streams.

The square in the top plot of Fig. 1 is CD -80 328 and has a photometric metallicity of -1.98 dex. It is not in the Beers & Sommer-Larsen (1995) nor Chiba & Yoshii (1998) catalogues. Its very low metallicity is spectroscopically confirmed by Beers et al. (1999) to be -2.09 dex. Its kinematics, $(U, V, W)_{GSR} = (-193, 117, 303)$ km s^{-1}, and metallicity suggest it could be a member of the H99b stream moving towards the NGP. However, its kinetic energy is too large to be consistent with the energies of the other members of the stream (listed in table 7 of Chiba & Beers 2000 and the energies were calculated using table 4 of Beers et al. 2000). Therefore, we consider this star to be a possible outlier, like the different outlier found by H99b. The red dots in the bottom plot of Fig. 1 apparently align in a linear structure. The mode of their photometric metallicities (-0.6 dex) agrees with the second group of tidal debris found by Helmi et al. (2006). However, the younger and wider age distribution of the linear structure argues against a tidal origin, suggesting a chance alignment is more probable.

The lack of strong clumping and apparent smoothness of the distribution in Fig. 1 suggests there are not any significant, coherent tidal streams in the sample (the tidal debris identified by Helmi et al. 2006 does not manifest itself in coherent tidal streams). The Helmi et al. (2006) APJ-space analysis of the CORAVEL dwarfs is similar to the H99a entropy technique (also used in H99b), since it partitions the parameter space and counts the number of stars in each cell. Therefore, we do not re-apply these techniques to the CORAVEL dwarfs in Fig. 1. In addition, these techniques cannot be applied to RAVE data as so far we have not derived accurate distances to RAVE stars (see Section 4). Instead, we apply the RAVE data analysis technique employed in Section 4 to the CORAVEL samples, in order to characterize the solar neighbourhood W distribution and to allow comparison between the CORAVEL and RAVE results. First, the next section demonstrates that RAVE data can be used on an equal footing with the CORAVEL data.
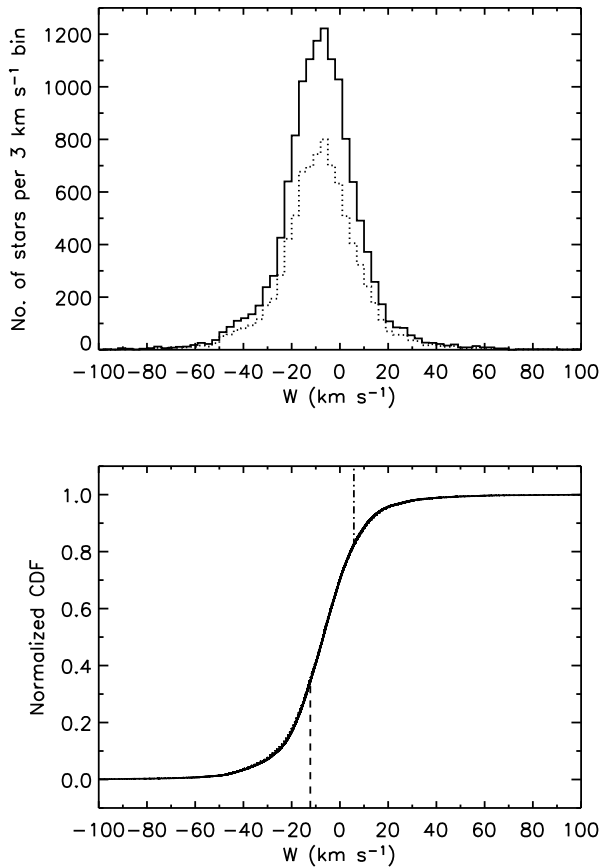
Figure 2. *Top:* W distribution of the CORAVEL dwarfs: all the 13 240 stars (solid histogram) and the 8589 single stars (dotted histogram). The 3 km s^{-1} velocity bin sizes are chosen to be twice the average space velocity error. *Bottom:* Normalized CDF of all the 13 240 CORAVEL giants (solid line) and the 8589 single stars (dotted line) as a function of W, where the maximum differences between them are indicated by vertical lines: D_+ (dot-dashed line) and D_- (dashed line).

2.3 Effect of Binarity on W velocity distribution

A double correlation peak may identify a spectroscopic binary from a single RV measurement but an average of more than four Geneva-Copenhagen observations are available per CORAVEL dwarf, allowing N04 to identify 3223 stars (out of 16 682, 19 per cent) as spectroscopic binaries of all kinds. If the velocities can be properly assigned to the two binary components, the centre-of-mass velocities of double-lined spectroscopic binaries can be computed by the method of Wilson (1941) without a full orbital solution. N04 provide systemic velocities of double-lined spectroscopic binaries where possible, otherwise the raw average RV is given for CORAVEL dwarfs, including single-lined spectroscopic binaries.

The average scatter of individual RVs of single-lined spectroscopic binaries, which have orbital periods of years or less, is ∼15 km s^{-1}. This scatter is an order of magnitude larger than the average error in each space velocity component of 1.5 km s^{-1}. Therefore, the mean RV of a single-lined spectroscopic binary may be more representative of the in-

stantaneous radial component of the orbital motion in the binary system than its systemic line-of-sight motion in the Galaxy, resulting in inaccurate and even potentially misleading space velocities.

Although any individual space velocity could be unreliable due to binarity, the statistical effect of binarity on the velocity distribution function of a large number of stars has not been empirically constrained before. This is due to the sparsity of RV data available with sufficient temporal coverage to generate good binarity detection statistics. The Geneva-Copenhagen survey is the largest, homogeneous RV survey with repeat measurements: 62 993 new RV observations of 13 464 programme stars, representing ∼1000 nights of data. Observations typically cover a time span of 1-3 years but some extend over a decade or more, allowing the majority of binaries to be identified.

The statistical effect of binarity on the velocity distribution function is investigated for the first time here because it has fundamental implications for our aims in this paper, as well as the observational strategies and science of on-going RV surveys. The vast majority of RAVE (and SEGUE) stars have never been spectroscopically observed before and RAVE (and SEGUE) observes most of them only once. Ideally kinematic studies should use centre-of-mass velocities but when these are not available, it is important to know how sensitive the analysis is to the kinematic affects of binarity.

We investigate the kinematic effect of binarity by comparing the W velocity distribution function of all the CORAVEL dwarfs, including binaries, to the corresponding distribution function of single stars (see top of Fig. 2). N04 provide a catalogue flag (f_b) that identifies confirmed or suspected binaries, where the information can come from one or several sources such as photometry, RV or astrometry. They identified 3537 visual binaries (out of 16 682 stars, 21 per cent) and the majority of systems with periods below 1000 days should be flagged. Single stars, for which the derived space velocities are more reliable, are defined by N04 as having a null f_b catalogue entry (8589 stars out of the 13 240 with space velocities, 65 per cent). Some CORAVEL dwarfs only have two observations. Accordingly, some long-period and/or low-amplitude binary stars will not be identified by the f_b flag and will thus be present in the sample of single stars. Their effect should be negligible compared to a bona fide sample of single stars due to the small amplitude of their orbital velocities.

Kepley et al. (2007) were able to use a parametric test (the Shapiro-Wilk test for deviations from normality) to search for streams in their stellar halo sample because the halo velocity distribution is approximated by a Gaussian. Both W velocity distribution functions in the top of Fig. 2 approximately consist of the sum of three Gaussians. These represent the young thin disc, where $\sigma_W \sim$ 10-15 km s^{-1}, the old thin disc, where $\sigma_W \sim$ 15-20 km s^{-1}, and the thick disc, where $\sigma_W > 30$ km s^{-1} (Seabroke & Gilmore 2007). The shape of the resulting distribution is a Gaussian with positive kurtosis (leptokurtic): it is more peaked and has heavier tails than a single Gaussian. This means a non-parametric statistical comparison test is required.

A standard distribution-free test is the Kolmogorov-Smirnov (K-S) test. The K-S statistic is the maximum difference over all values of a single, independent variable x

of two cumulative distribution functions (CDFs). However, the sensitivity of the K-S test is not independent of x: it tends to be most sensitive around the median value and less sensitive at the extreme ends of the distribution. Identifying the points at $\pm\infty$ (wrapping the x-axis around a circle) guarantees equal sensitivities at all values of x. This is an invariant K-S test called the Kuiper test (Press et al. 1992). For comparing two different CDFs, the Kuiper statistic, defined as

$$D = D_+ + D_-, \tag{7}$$

is the sum of the differences between the CDFs, where

$$D_+ = \max[S_{N_1}(x) - S_{N_2}(x)] \tag{8}$$

and

$$D_- = \max[S_{N_2}(x) - S_{N_1}(x)], \tag{9}$$

where $S_{N_i}(x)$ is the function giving the fraction of data points $\leqslant x$. The statistical significance of D, $P(D > \text{observed}) = Q(\lambda)$ is given by

$$Q = 2\sum_{j=1}^{\infty}(4j^2\lambda^2 - 1)e^{-2j^2\lambda^2}, \tag{10}$$

where Q is a monotonic formula with variable j for the asymptotic behaviour of the statistic D, satisfying $Q(0) = 1$ and $Q(\infty) = 0$, where

$$\lambda = D\left(\sqrt{N_e} + 0.155 + \frac{0.24}{\sqrt{N_e}}\right) \tag{11}$$

and

$$N_e = \frac{N_1 N_2}{N_1 + N_2}. \tag{12}$$

To compare all the CORAVEL dwarfs ($N_1 = 13\ 240$) with the single-star CORAVEL dwarfs ($N_2 = 8589$), $x = W$ in equations 8 and 9, giving $D_+ = 0.004$, $D_- = 0.009$ (see bottom of Fig. 2) and $D = 0.013$. The sample size is sufficiently large ($N_e = 5209.51$) to give the test enough power to detect significant differences and reject the null hypothesis (that all the stars and the single stars are drawn from the same parent population) if it is false. $Q = 0.887$, signifying the data fail to reject the null hypothesis. This means that, statistically, stellar binarity does not affect the W distribution of the CORAVEL dwarfs significantly.

Because binaries are, on average, apparently brighter than single stars, binaries are abundant in apparent magnitude limited samples like the Geneva-Copenhagen survey. The Kuiper test suggests we can safely include binaries, nearly doubling the sample size of the CORAVEL dwarfs and increasing the power of the test. This means the RAVE RVs, which includes binaries, can be used on an equal footing with the CORAVEL data. Fig. 3 shows that including binaries does not increase the local volume of the solar neighbourhood sampled by the CORAVEL dwarfs.

2.4   Determining W_{LSR} for the CORAVEL dwarfs

To search for streams, a Kuiper test could be used to compare the W distribution of the CORAVEL dwarfs with a Cauchy-Lorentz distribution (heavy-tailed Gaussian). Its peak location (x_0) and half-width at half-maximum scale
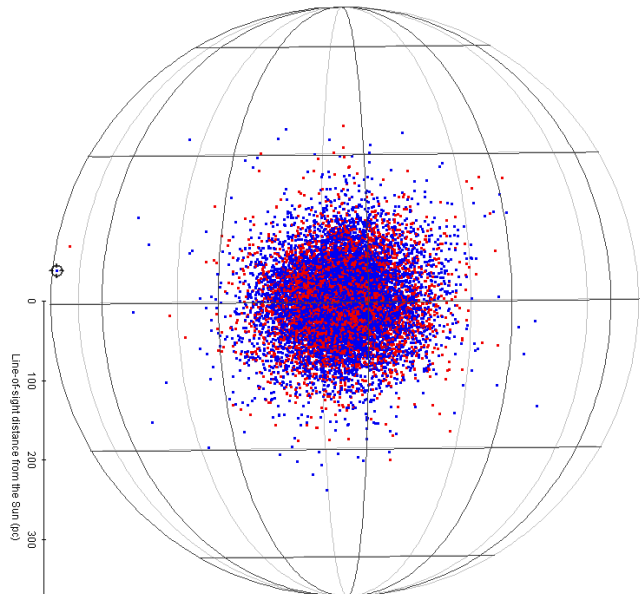

Figure 3. Three dimensional sky distribution of all the 13 240 CORAVEL dwarfs with W velocities (red) and the 8589 single-star CORAVEL dwarfs (blue). The spherical polar axes have a radius of 370 pc, centred on the Sun, chosen to include the most distant CORAVEL dwarf with a W velocity (363 pc, marked by the black cursor). The viewer is in the Galactic plane, inside the solar circle at $l \sim 30°$ (the Galactic centre is over the viewer's left shoulder). The nearest line of constant l is $l = 30°$ (with the majority of the stars behind it). l increases to the right (anticlockwise) with lines of constant l every $30°$. All the lines of constant l converge at the NGP ($b = +90°$, top) and at the SGP ($b = -90°$, bottom), with lines of constant b every $30°$.

(γ) parameters could be theoretically determined according to the Galactic volume sampled and the age-velocity dispersion relation of the thin and thick discs. However, the functional form of these relations remains uncertain (Seabroke & Gilmore 2007). In addition, the test hypothesis would be whether the data is exactly a Cauchy-Lorentz distribution with the specified x_0 and γ. The hypothesis could be rejected due to the data having a slightly different x_0 and γ than those specified. Thus, the test may not be very sensitive to the presence of streams.

A more straight-forward approach is to test the symmetry between the two halves of the W distribution. In-falling streams on to the Milky Way disc will reveal themselves as overdensities in the distribution of W with respect to the Galactic plane. W is positive towards the NGP and negative towards the SGP (symbolically denoted $+W$ and $-W$ respectively for brevity), so a stream falling onto the Galactic disc from the NGP ('above' the Galactic plane) would have $-W$ and a stream falling onto the Galactic disc from the SGP ('below' the plane) would have $+W$. A stream falling through the disc from the NGP to SGP would exhibit $-W$ both above and below the plane and $+W$ both above and below the plane falling from the SGP to the NGP. A symmetry test between the two sides of the W distribution, if sensitive enough to the number of stream stars, will find the asymmetry caused by a single stream.

W is measured relative to the Sun. The top of Fig. 2 shows that the W distribution is not centred on zero velocity.
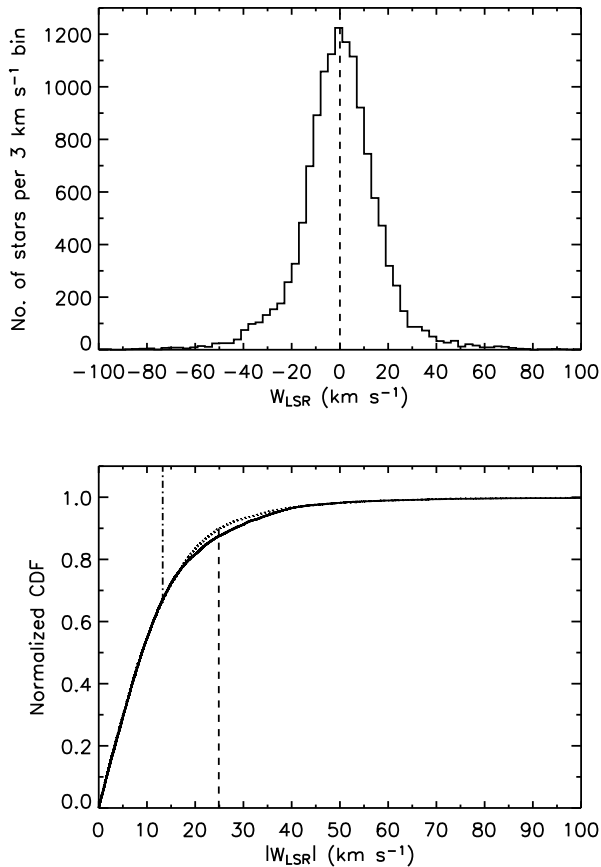
Figure 4. *Top:* W_{LSR} distribution of the CORAVEL dwarfs (solid histogram) either side of the $W_{LSR} = 0$ dividing line (dashed line). *Bottom:* Normalized CDF of $W_{LSR} < 0$ (solid line) and $W_{LSR} > 0$ (dotted line), showing D_- (dashed line) and D_+ (dot-dashed line).

The Kuiper test is sensitive to the sign of the W velocities (see bottom of Fig. 2) so the absolute values of $-W$ velocities are required to compare them to $+W$ to test the symmetry of the distribution. The easiest method to implement this Kuiper symmetry test is to transform the heliocentric reference frame to one centred on zero velocity – the LSR reference frame, where $W_{LSR}^\odot$ in equation 6 is the centre of the W distribution in the top of Fig. 2. $W_{LSR}^\odot$ needs to be determined to apply its correction to the W distribution to convert it to a W_{LSR} distribution.

We determine $W_{LSR}^\odot$ by varying its value in the Kuiper symmetry test to find the best agreement between the two halves of the resulting W_{LSR} distribution (minimum value of D). D is calculated using equations 8 and 9 but now $x = |\pm W_{LSR}|$. The maximum differences between $S_{N_{W_{LSR}<0}}(|-W_{LSR}|)$ and $S_{N_{W_{LSR}>0}}(+W_{LSR})$ are calculated over the range $0 < |\pm W_{LSR}| < \infty$. The top of Fig. 4 shows the W_{LSR} distribution for the minimum value of D, where $W_{LSR}^\odot = 7.0$ km s^{-1} to the nearest 0.1 km s^{-1}. Our value of $W_{LSR}^\odot$ also agrees within the errors with the Dehnen & Binney (1998) measurement: $W_{LSR}^\odot = 7.17 \pm 0.38$ km s^{-1} (see Appendix A for further discussion on the determination of $W_{LSR}^\odot$ and historical parallels).

Having determined $W_{LSR}^\odot$, we continue to vary its value

until a 4σ statistically significant difference ($Q < 6 \times 10^{-5}$) is generated between the two halves of the resulting W_{LSR} distribution to gauge how sensitive the Kuiper symmetry test is to the measured value of $W_{LSR}^\odot$. Table 1 shows that $W_{LSR}^\odot$ can be placed -1.4 km s^{-1} from our measured value of $W_{LSR}^\odot$ in the $-W_{LSR}$ distribution, whereas it can only be placed less than half that speed ($+0.6$ km s^{-1}) from our measured value of $W_{LSR}^\odot$ into the $+W_{LSR}$ distribution. This is because the position of $W_{LSR}^\odot$ is sensitive to the slight asymmetry due to D_+ in the bottom of Fig. 4 at $|W_{LSR}| = 13$ km s^{-1}. Although it may not appear so in the top of Fig. 4 because of the binning, there are more stars with $0 < W_{LSR} \leqslant 13$ than $-13 < W_{LSR} \leqslant 0$ km s^{-1}. However, $S_{N_{W_{LSR}<0}}(|-W_{LSR}|) > S_{N_{W_{LSR}>0}}(+W_{LSR})$, allowing the line of symmetry ($W_{LSR}^\odot$) to be placed further into the $-W_{LSR}$ distribution than the $+W_{LSR}$ distribution. If the position of $W_{LSR}^\odot$ was sensitive to the larger asymmetry due to D_- in the bottom of Fig. 4 at $|W_{LSR}| = 25$ km s^{-1}, the reverse would be true i.e. even though there are more stars with $0 < W_{LSR} \leqslant 25$ than $-25 < W_{LSR} \leqslant 0$ km s^{-1}, $S_{N_{W_{LSR}>0}}(+W_{LSR}) > S_{N_{W_{LSR}<0}}(|-W_{LSR}|)$, which would allow the line of symmetry ($W_{LSR}^\odot$) to be placed further into the $+W_{LSR}$ distribution than the $-W_{LSR}$ distribution. This demonstrates that $W_{LSR}^\odot$ is only sensitive to asymmetries at $|W_{LSR}| < \sigma_{W_{LSR}}$ (in this case D_+ rather than D_-), despite $D_+ << D_-$.

$W_{LSR}^\odot$ of the full sample of CORAVEL dwarfs coincides with the mode of the W_{LSR} distribution in the top of Fig. 4. This suggests that there cannot be many CORAVEL dwarfs with $|W_{LSR}| < \sigma_{W_{LSR}}$ belonging to vertically coherent streams with systemic W_{LSR} velocities. If there were, they would have biased the measurement of $W_{LSR}^\odot$ away from the mode.

A coherent stream with a systemic space velocity would be visible as an overdensity in the CORAVEL dwarf $U-W$ and $V-W$ space diagrams. These diagrams in fig. 20 in N04 do not exhibit any such vertical substructure. In fact, Seabroke & Gilmore (2007) show the CORAVEL dwarfs are well phase-mixed vertically because of the sample's low scaleheight (see Fig. 3). This suggests there are no vertically coherent streams currently passing through the solar neighbourhood, in agreement with the lack of strong clumping in Fig. 1.

2.5 Sensitivity of the W_{LSR} symmetry of the CORAVEL dwarfs to tidal streams

In this section, we investigate the sensitivity of the W_{LSR} symmetry of the CORAVEL dwarfs to tidal streams at $|W_{LSR}| \geqslant \sigma_{W_{LSR}}$. The previous section suggests the sample of CORAVEL dwarfs is free from vertically coherent streams. This means its distribution can be used as a smooth background against which we can investigate the effect of a tidal stream passing vertically through the solar neighbourhood. We do this by simulating a stream, pseudo-randomly generating a Gaussian with $\sigma_s = 10$ km s^{-1}, and adding it to the sample. This dispersion was chosen because the best studied tidal stream in the literature, the Sgr stream, is found to be dynamically cold by two different groups: Majewski et al. (2004) used medium-resolution spectroscopy to find an intrinsic dispersion of $\sigma = 10.4 \pm 1.3$

Table 1. Results of the Kuiper symmetry test, applied to the CORAVEL dwarfs, to determine $W^{\odot}_{LSR}$ to the nearest 0.1 km s^{-1}, where $\Delta W^{\odot}_{LSR} = W^{\odot}_{LSR} - 7.0$ km s^{-1}.

$W^{\odot}_{LSR}$	$\Delta W^{\odot}_{LSR}$	$N_{W_{LSR}<0}$	$N_{W_{LSR}>0}$	N_e	D_-	D_+	D	Q
5.6	−1.4	7176	6064	3287	0.0484	0.0021	0.0505	3×10^{-6}
7.0	0.0	6583	6657	3310	0.0250	0.0064	0.0314	0.0341
7.6	0.6	6334	6906	3304	0.0242	0.0212	0.0454	6×10^{-5}

km s^{-1} (after removing random errors of ~5.3 km s^{-1}); and Monaco et al. (2007) fitted a Gaussian of $\sigma = 8.3 \pm 0.9$ km s^{-1} to their sample of high-resolution spectroscopically derived RVs.

To investigate how sensitive the Kuiper symmetry test is to the choice of σ_s, we repeated the above experiment with $\sigma_s = 3$ and 17.3 km s^{-1}. These dispersions are physically motivated: H99a state that the intrinsic dispersion for a tidal stream from a Large Magellanic Cloud-type progenitor is ~3-5 km s^{-1} after a Hubble time; and Duffau et al. (2006) discovered the Virgo stellar stream with $\sigma = 17.3$ km s^{-1}. We find that the number of stars required to generate a 4σ tidal stream detection is relatively insensitive to σ_s. The conservation of phase-space density results in σ decreasing as 1/time at each point along a stream (H99a). Hence, the ability of the test to detect a stream is not biased by the dynamical age of the stream.

The simulated tidal stream is added to the sample of CORAVEL dwarfs at $W = \pm(1, 2, 3, \sim13)\sigma_{W_{LSR}}$, where $\sigma_{W_{LSR}} \approx 18$ km s^{-1}, to test the sensitivity of the W_{LSR} symmetry to the presence of each stream. Approximately $-13\sigma_{W_{LSR}}$ corresponds to $W_{LSR} \approx -242$ km s^{-1} calculated by Freese et al. (2004) using the eight clump stars from Chiba & Yoshii (1998) in the H99b stream (the CORAVEL dwarfs with W_{LSR} nearest to this value are at -286 and -179 km s^{-1}).

At each position, the random population of the simulated tidal stream is increased until it causes the Kuiper symmetry test to reject the null hypothesis (that $W_{LSR} < 0$ and $W_{LSR} > 0$ are drawn from the same parent population) at the 4σ statistical significance level. The test results in Table 2 are indicative because they represent a single realization of a pseudo-random Gaussian added to the sample and we have not conducted a full Monte Carlo simulation. Nevertheless, the indication that more tidal stream stars are required to generate a 4σ tidal stream detection at 2 and $3\sigma_{W_{LSR}}$ than at -2 and $-3\sigma_{W_{LSR}}$ seems plausible due to the asymmetry already in the W_{LSR} distribution: D_- in the bottom of Fig. 4 at $|W_{LSR}| = 25$ km s^{-1}. Placing streams in the $-W_{LSR}$ distribution, further increases D_- and decreases D_+. The reverse is true for placing streams in the $+W_{LSR}$ distribution but even more stream stars are required to cancel out the intrinsic D_- and increase D_+ to the 4σ statistical significance level (see Fig. 5).

The test becomes more sensitive (less stream stars required to generate a 4σ detection), the further a stream is from the centre of the distribution. However, Table 2 shows that the number of stream stars required for a 4σ detection stays approximately constant (saturates) at $\leqslant -3\sigma_{W_{LSR}}$. This is because the positions of D_- and D_+ have become fixed and their values saturated, whereas D_+ is still sensitive
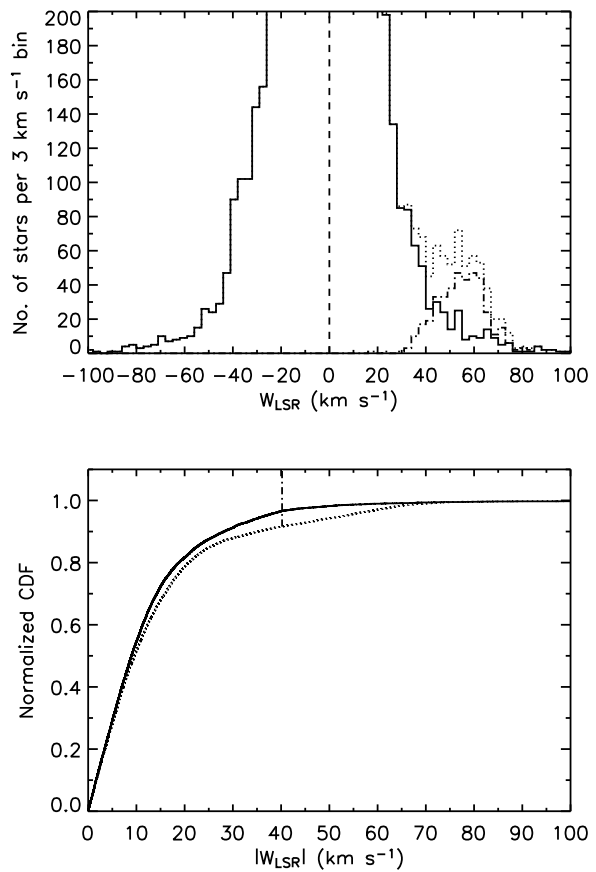

Figure 5. *Top:* W_{LSR} distribution of the CORAVEL dwarfs (solid histogram) either side of the $W_{LSR} = 0$ dividing line (dashed line). The pseudo-randomly generated Gaussian (representing a $\sigma = 10$ km s^{-1} tidal stream) included in the data set (dotted histogram) that caused the Kuiper symmetry test to reject the null hypothesis at 4σ when placed at $3\sigma_{W_{LSR}}$ is also plotted separately (dot-dashed line). *Bottom:* Normalized CDF of $W_{LSR} < 0$ (solid line) and $W_{LSR} > 0$ (dotted line), showing D_+ (dot-dashed line). D_- is not visible in this plot at $|W_{LSR}| \approx 0$.

to perturbation at $W_{LSR} > 3\sigma_{W_{LSR}}$ by hundreds of stream stars.

H99a demonstrate that phase-mixing allows different tidal streams from a single disrupted object to be observed with opposite motion in the vertical direction (e.g. the two H99b streams). If two such streams contain similar numbers of stars, the Kuiper symmetry test may not find them because their presence may not create enough of an asymmetry between the two sides of the W distribution. H99a predict inside a 1 kpc^3 volume centred on the Sun, there should be

Table 2. Results of the Kuiper symmetry test, applied to the CORAVEL dwarfs, to determine the approximate number of tidal stream stars (N_s) required, in pseudo-randomly generated $\sigma_s = 10$ km s^{-1} Gaussians, placed at $\pm(1, 2, 3, \sim13)\sigma_{W_{LSR}}$ in the W_{LSR} distribution, to cause the test to reject the null hypothesis at 4σ ($Q < 6 \times 10^{-5}$). $\% = N_s/(N_s + N_{total})$ where $N_{total} = 13$ 240. ρ_s is the stellar density of each stream, in $N \times 10^6$ stars kpc^{-3}, calculated by dividing the N_s of each stream by the volume within which the CORAVEL dwarfs are complete, approximated by a sphere with radius $\sim$40 pc ($\sim3\times10^{-4}$ kpc^{-3}).

$\sigma_{W_{LSR}}$	N_s	%	ρ_s	$N_{W_{LSR}<0}$	$N_{W_{LSR}>0}$	N_e	D_-	D_+	D	Q
-1	600	4.3	2.2	7165	6675	3456	0.0414	0.0033	0.0447	5×10^{-6}
1	500	3.6	1.9	6601	7139	3430	0.0163	0.0339	0.0502	2×10^{-6}
-2	200	1.5	0.7	6783	6657	3360	0.0469	0.0010	0.0479	1×10^{-5}
2	400	2.9	1.5	6583	7057	3406	0.0026	0.0458	0.0484	7×10^{-6}
-3	200	1.5	0.7	6783	6657	3360	0.0508	0.0004	0.0512	1×10^{-6}
3	400	2.9	1.5	6583	7057	3406	0.0026	0.0504	0.0530	3×10^{-7}
~-13	200	1.5	0.7	6783	6657	3360	0.0508	0.0004	0.0512	1×10^{-6}
~13	300	2.2	1.1	6583	6957	3382	0.0036	0.0445	0.0481	9×10^{-6}

300-500 tidal streams containing a few hundred stars each if the whole stellar halo was built up by disrupting satellites. However, neither the CORAVEL nor RAVE surveys provide complete coverage of this volume and so are very incomplete with respect to halo stars. Thus, if these streams exist in our samples, they will most likely contain fewer stars than the detection thresholds of the Kuiper symmetry test in Table 2. This means the test is not sensitive to these streams, regardless of their possible symmetries. The number of stars required for a detection suggests the test is better suited to detect less phase-mixed, more coherent streams in configuration space, like the Sgr streams that contain hundreds of stars.

Seabroke & Gilmore (2007) estimated that are $\sim$1300 CORAVEL dwarfs in the Hercules dynamical stream. This substructure corresponds to 10 per cent of the sample and is easily visible in the N04 $U-V$ space diagram (their fig. 20). F05 show in their sample of CORAVEL giants that the Hercules stream has $\sigma_U = 28.35 \pm 1.68$ and $\sigma_V = 9.31 \pm 1.22$ km s^{-1}. More than halving σ_U would also more than halve the number of Hercules stars, bringing them into agreement with the numbers in Table 2 but its nucleus would still be discernible as an overdensity in the N04 $U-V$ space diagram.

The high number of stream stars needed to cause a statistically significant asymmetry would most likely be visible as substructure in the N04 $U-W$ and $V-W$ space diagrams and strong clumping in Fig. 1. Given this and the symmetry of the W_{LSR} distribution, we conclude that it is unlikely that the sample of CORAVEL dwarfs contains any vertically coherent streams consisting of $\gtrsim$200 stars. Veltz et al. (2007) find the scaleheight of the thin disc is $\sim$225 pc so the CORAVEL dwarfs only sample a very local volume of the thin disc (N04 showed the local thick disc consists of $<$10 per cent of the sample).

F-G turnoff stars are a good indicator of stellar number density. The only part of the Sgr stream close enough to the Sun where this quantity can be reliably measured is 50 kpc from the Sgr dSph (SDSS Stripe 82). Freese et al. (2005) estimate the full-width at half-maximum of the Sgr stream in Stripe 82 is 4-8 kpc, which is consistent with $\sigma \approx 2$ kpc, derived from 2MASS M giants in the stream (Majewski et al. 2003). Freese et al. (2005) use this stream width to estimate its stellar density: 210-740 stars kpc^{-3}. They use Blue Horizontal Branch stars in Stripe 82 and in another part of the

stream, also 50 kpc from the Sgr dSph (Stripe 10), to estimate how stellar density varies as a function of position along the stream and find the variation is a factor of 1-2, implying the stellar density of the Sgr stream in the solar neighbourhood is in the range of 210-1480 stars kpc^{-3}. An upper limit on the stream density of $1.6 \times 10^4 M_\odot$ kpc^{-3} is derived from the models shown in Martínez-Delgado et al. (2007), assuming all the mass in the Sgr dSph is in the form of stars.

The CORAVEL dwarfs are volume complete out to $\sim$40 pc, which corresponds to a spherical volume of $\sim3 \times10^{-4}$ kpc^3. Therefore, even the upper bound on the number of Sgr stream stars expected to be passing through this volume is $<$1. Fig. 3 illustrates that there are a significant number of stars out to $\sim$100-200 pc so if the Sgr stream is passing through the spherical CORAVEL dwarf volume (radius $\sim$200 pc), only of order unity CORAVEL dwarfs are likely to be Sgr stars. Table 2 shows that the Kuiper symmetry test is not sensitive to such a small number of stream stars so if there is subtle clumping in Fig. 1 the test would not find such weak streams.

From fig. 1 of Fuchs et al. (2006), we estimate that at $Z \sim 2$ kpc, the VOD minus the vertical density profile at the position of the Sun of a smooth Galaxy model is 1.2 $\times10^5$ stars kpc^{-3} in the 13-h CADIS field. Therefore, if this structure exists in the solar neighbourhood with this density, there will not be many more than 30-40 CORAVEL dwarfs belonging to it. Table 2 shows that the Kuiper symmetry test is not sensitive to such a small number of stars. The table illustrates that even the smallest number of stars required for a stream detection in this sample only puts a very weak constraint on the stellar density of a coherent structure in the solar neighbourhood with vertically coherent kinematics.

3 CORAVEL GIANTS

3.1 Derivation of the space velocities of the CORAVEL giants

The F05 sample of CORAVEL giants is the intersection of several data sets: (i) spectral types K and M in the *Hipparcos* catalogue; (ii) proper motions from the *Tycho-2* catalogue; (iii) CORAVEL RVs for stars in list (i) in the Northern hemisphere ($\delta > 0°$), observed with the Swiss 1-m telescope

at Observatoire de Haute-Provence, France. The *Hipparcos* parallaxes were used to construct a crude Hertzsprung-Russell (H-R) diagram from which dwarfs were identified and removed from the sample. Stars with peculiar spectra, such as T Tau stars, Mira variables and S stars were eliminated using diagnostics based on RV variability and CORAVEL cross-correlation profiles, combined with literature searches. Binaries for which no centre-of-mass RV could be estimated were removed using the F05 binarity flag (B). A star was excluded from their (and our) kinematic analysis if it is a spectroscopic binary ($B = 0$) or a visual binary with no orbit available ($B = 5$) or an uncertain case, either a spectroscopic binary or supergiant ($B = 3$) or for a visual binary ($B = 8$), leaving 6030 stars (5311 K and 719 M giants).

Because the CORAVEL giants are at distances approximately an order of magnitude greater than the CORAVEL dwarfs, the σ_π/π distribution for the giants is correspondingly less accurate than that for the dwarfs. This means, unlike for the dwarfs, simple inversion of the parallaxes of the giants results in biased estimates of their distances for the >3000 giants with $\sigma_\pi/\pi > 20$ per cent (Brown et al. 1997). To derive bias-free distances for all the CORAVEL giants, F05 used the Bayesian Luri-Mennessier maximum-likelihood method (Luri et al. 1996) to model the sample in order to assign each star to a kinematic 'base' group. Given the maximum-likelihood estimator of its assigned group parameters and its observed values, F05 obtain the marginal probability density law for the distance of each star from the global probability density function. These distances were used with the CORAVEL RVs and *Tycho-2* proper motions to derive the space velocities.

3.2 Orbital angular momenta of the CORAVEL giants

Fig. 6 shows that, despite probing a larger volume than the CORAVEL dwarfs, the giants, unlike the dwarfs, do not include a symmetric (no net rotation) halo sample. This figure includes all the sample and thus none of the CORAVEL giants are members of the H99b streams. The F05 dynamical streams are part of the smooth distribution in Fig. 6 because all the stars exhibit a similar range of thin disc J_Z values. The lack of strong clumping again suggests there are not any coherent tidal streams in the sample.

3.3 Determining W_{LSR} for the CORAVEL giants

This section repeats the technique applied to the CORAVEL dwarfs in Section 2.4 to the CORAVEL giants. The top of Fig. 7 shows the W_{LSR} distribution for the minimum value of D, where $W_{LSR}^\odot = 7.0$ km s^{-1} to the nearest 0.1 km s^{-1}. This is the same value as found for the CORAVEL dwarfs. In the reverse situation to the dwarfs, $W_{LSR}^\odot$ for the giants can be placed further in the $+W_{LSR}$ distribution than the $-W_{LSR}$ distribution. The placement is twice as far as the maximum $W_{LSR}^\odot$ position for the dwarfs. This shows the position of $W_{LSR}^\odot$ for the giants is now sensitive to the slight asymmetry due to D_- in the bottom of Fig. 7 at $|W_{LSR}| = 24$ km s^{-1} because D_+ is at the centre of the distribution.

$W_{LSR}^\odot$ is in agreement with the mode of the W_{LSR} distribution in Fig. 7. Again, this suggests that there cannot
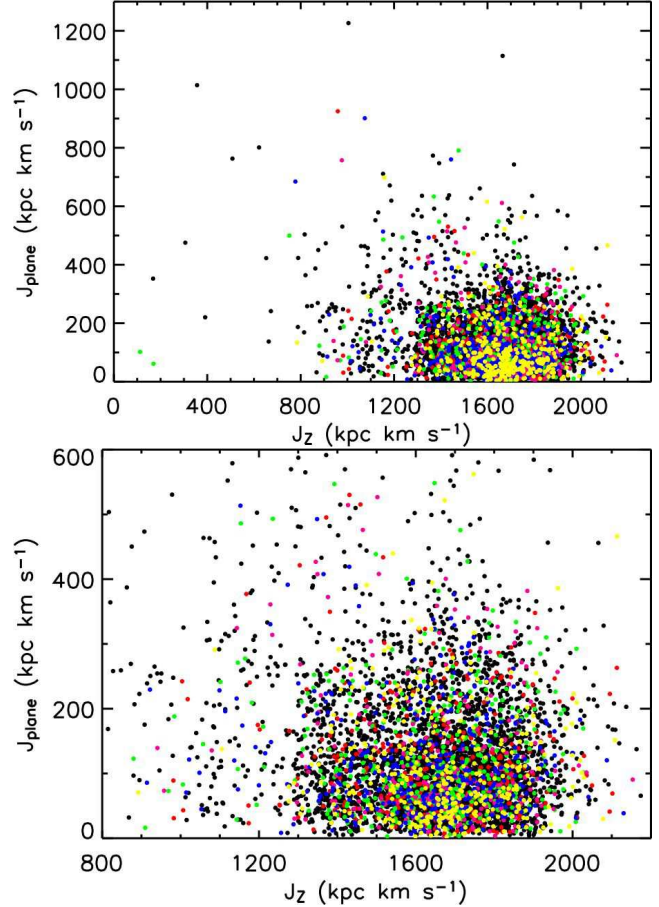

Figure 6. Distribution of CORAVEL giants in the plane of orbital angular momentum components, colour-coded according to the F05 maximum likelihood base group assignment to known kinematic features of the solar neighbourhood: smooth background (black), Sirius moving group (magenta), young kinematics (yellow), Hyades-Pleiades supercluster (red), Hercules stream (green) and high-velocity stars (blue). Note the different scale between the top plot above and in Fig. 1.

be many stars belonging to vertically coherent streams with systemic W_{LSR} velocities. If there were, they would have biased the measurement of $W_{LSR}^\odot$ away from the mode. Table 3 shows the value of D_- for the giants is greater than for the dwarfs and so the value of D is also larger for the giants than for the dwarfs. In spite of this, the Q value for the giants is less significant than for the dwarfs because the N_e value for the giants is half the value for the dwarfs. Hence, the D_- asymmetry does not bias the $W_{LSR}^\odot$ value for the giants.

3.4 Sensitivity of W_{LSR} symmetry of the CORAVEL giants to tidal streams

This section repeats the technique applied to the CORAVEL dwarfs in Section 2.5 to the CORAVEL giants, except the dispersion of the giants is slightly larger: $\sigma_{W_{LSR}} \approx 19$ km s^{-1}. Table 4 shows that, because D_+ is at the centre of the distribution, many more stream stars are required to cause D_+ to generate a 4σ stream detection at $W_{LSR} = 1\sigma_{W_{LSR}}$ than at $-1\sigma_{W_{LSR}}$. As before, the test becomes more sensitive (less stream stars required to generate a 4σ detection),

Table 3. Results of the Kuiper symmetry test, applied to the CORAVEL giants, to determine $W^\odot_{LSR}$ to the nearest 0.1 km s^{-1}, where $\Delta W^\odot_{LSR} = W^\odot_{LSR} - 7.0$ km s^{-1}.

$W^\odot_{LSR}$	$\Delta W^\odot_{LSR}$	$N_{W_{LSR}<0}$	$N_{W_{LSR}>0}$	N_e	D_-	D_+	D	Q
5.4	−1.6	3397	2633	1483	0.0609	0.0082	0.0691	3×10^{-5}
7.0	0.0	3127	2903	1505	0.0316	0.0081	0.0397	0.1415
10.4	3.4	2589	3441	1477	0.0016	0.0677	0.0693	3×10^{-5}

Table 4. Results of the Kuiper symmetry test, applied to the CORAVEL giants, to determine the approximate number of tidal stream stars (N_s), required in pseudo-randomly generated $\sigma_s = 10$ km s^{-1} Gaussians, placed at $\pm(1, 2, 3, \sim13)\sigma_{W_{LSR}}$ in the W_{LSR} distribution, to cause the test to reject the null hypothesis at 4σ ($Q < 6 \times 10^{-5}$). $\% = N_s/(N_s + N_{total})$ where $N_{total} = 6030$. ρ_s is the stellar density of each stream, in N stars kpc^{-3}, calculated by dividing the N_s of each stream by the volume within which the CORAVEL giants are complete, approximated by a hemisphere with radius ~0.29 kpc (~0.05 kpc^{-3}).

$\sigma_{W_{LSR}}$	N_s	%	ρ_s	$N_{W_{LSR}<0}$	$N_{W_{LSR}>0}$	N_e	D_-	D_+	D	Q
−1	300	4.7	6000	3417	2913	1572	0.0604	0.0084	0.0688	1×10^{-5}
1	800	11.7	16 000	3153	3677	1697	0.0039	0.0665	0.0704	2×10^{-6}
−2	200	3.2	4000	3327	2903	1550	0.0772	0.0064	0.0836	3×10^{-8}
2	300	4.7	6000	3127	3203	1582	0.0052	0.0687	0.0739	2×10^{-6}
−3	200	3.2	4000	3327	2903	1550	0.0804	0.0064	0.0868	5×10^{-9}
3	200	3.2	4000	3127	3103	1557	0.0119	0.0678	0.0797	2×10^{-7}
~-13	200	3.2	4000	3327	2903	1550	0.0804	0.0064	0.0868	5×10^{-9}
~13	200	3.2	4000	3127	3103	1557	0.0119	0.0697	0.0816	7×10^{-8}

the further a stream is from the centre of the distribution. However, Table 4 shows that, again, the number of stream stars required for a 4σ detection stays approximately constant (saturates) at $\leqslant -3\sigma_{W_{LSR}}$ for the same reason as before.

The number of stream stars required in the dwarf sample are also needed in the giant sample at $W_{LSR} = 3\sigma_{W_{LSR}}$ to generate a 4σ detection (see Fig. 8). This is because the top of Fig. 9 shows that both samples include similar numbers of stars at $W_{LSR} = \pm 3\sigma_{W_{LSR}}$, even though the dwarf sample is twice as large as the giant one. The larger volume sampled by the giants (see Fig. 10) increases the numbers of giants in the tails of its W_{LSR} distribution. It is this greater volume, and correspondingly different stellar population mix, that makes the giant distribution differ from the dwarf one as seen in the bottom of Fig. 9.

Fig. 10 shows that the nine stars at ~4.55 kpc towards the NGP, proposed as a candidate halo stream by Majewski (1992), are not in the sample of CORAVEL giants. Majewski et al. (1994) measured the RVs of six out of the nine stars and H99a calculated their mean vertical velocity to be $\langle W \rangle = -76 \pm 18$ km s^{-1} and $\sigma_W = 35 \pm 24$ km s^{-1}. There are giants in the sample with these velocities but they do not share the angular momenta of these stars computed by H99a as $J_Z << 0$. This is far from the range in Fig. 6, suggesting none of the CORAVEL giants are members of this stream. We do not see any evidence of the more general halo streaming from the NGP towards the Galactic plane reported by Majewski et al. (1996) and Kinman et al. (2007). Kinman et al. (2007) speculated their streaming could be connected with the VOD.

The method briefly described in Section 3.1 allowed F05 to search for and characterize kinematic substructure in their sample. Their method identified three kinematic base groups: the Sirius moving group, giants with young kinemat-

ics and the Hyades-Pleiades supercluster. F05 found these groups have dispersions similar to cold streams ($\sigma_{U,V,W} \sim 5\text{-}10$ km s^{-1}). The smooth background contains more than an order of magnitude more stars than in each group. The groups are barely visible as overdensities against the background (see Seabroke & Gilmore 2007 fig. 3). Each contains similar numbers of stars (see table 2 in F05) to the numbers in Table 4 required for our Kuiper symmetry test to detect vertically coherent streams. F05 did not report any vertical substructure. This agrees with our Kuiper symmetry test results and the CORAVEL giants being well phase-mixed vertically (see Seabroke & Gilmore 2007 figs 4 and 5). This suggests the D_- asymmetry in Fig. 7 is not caused by a vertically coherent stream.

Approximately 80 per cent of the CORAVEL giants are Hipparcos 'survey' stars. Therefore, the sample is complete for the K and M giants brighter than $V = 7.3 + 1.1|\sin b|$ (Udry et al. 1997). This magnitude threshold translates into distances of 290 pc in the galactic plane and 480 pc in the direction of the galactic pole for a typical $M_V = 0$ giant. These values are, however, very sensitive to the adopted absolute magnitude. They become 45 pc for a subgiant with $M_V = +4$ in the galactic plane, and 2.9 kpc for a supergiant with $M_V = -5$ (e.g. the most luminous giants and supergiants colour-coded yellow in Fig. 10). We consider the volume within which the CORAVEL giants are complete to be approximated by a hemisphere with radius ~0.29 kpc (~0.05 kpc^{-3}).

From the Freese et al. (2005) arguments, we estimate that 10-80 Sgr stream stars could be within the volume where the CORAVEL giants are complete. A caveat against interpreting the D_- asymmetry as not due to a stream is that the numbers of stars found by F05 to be part of substructure are much larger than the expected number of Sgr and Majewski (1992) halo stream stars. This implies that
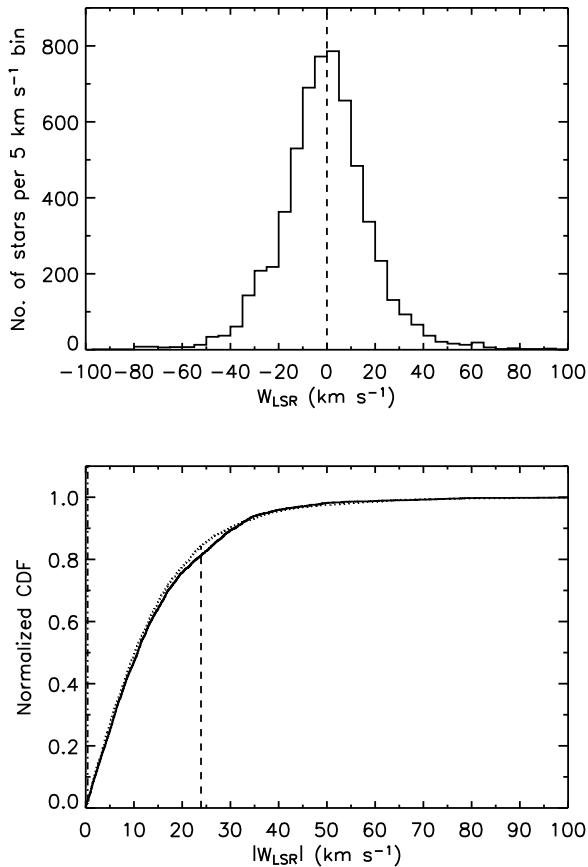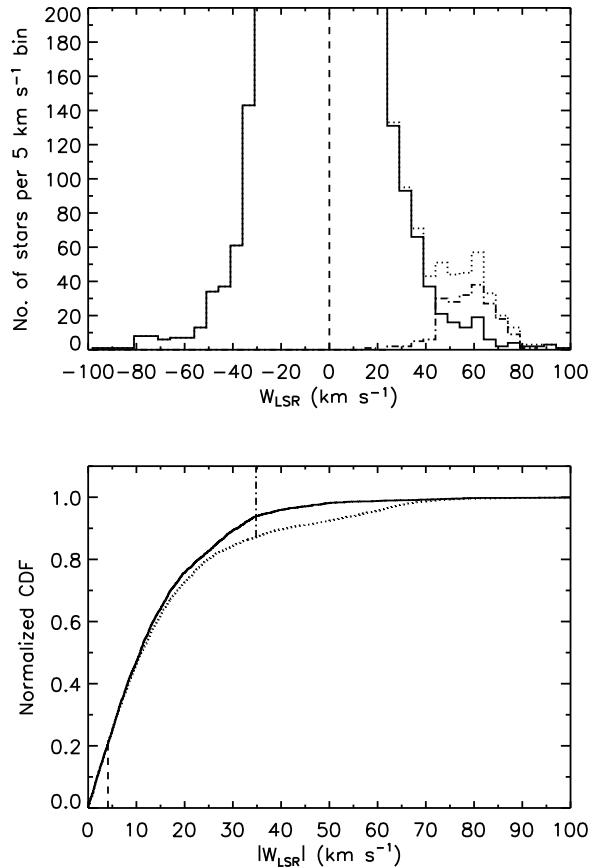
Figure 7. *Top:* W_{LSR} distribution of the CORAVEL giants (solid histogram) either side of the $W_{LSR} = 0$ dividing line (dashed line). The 5 km s^{-1} velocity bin sizes are chosen to be twice the average space velocity error. *Bottom:* Normalized CDF of $W_{LSR} < 0$ (solid line) and $W_{LSR} > 0$ (dotted line), showing D_{-} (dashed line) and D_{+} (dot-dashed line, just visible at $|W_{LSR}| \approx 0$).

Figure 8. *Top:* W_{LSR} distribution of the CORAVEL giants (solid histogram) either side of the $W_{LSR} = 0$ dividing line (dashed line). The pseudo-randomly generated Gaussian (representing a $\sigma = 10$ km s^{-1} tidal stream) included in the data set (dotted histogram) that caused the Kuiper symmetry test to reject the null hypothesis at 4σ when placed at $3\sigma_{W_{LSR}}$ is also plotted separately (dot-dashed line). *Bottom:* Normalized CDF of $W_{LSR} < 0$ (solid line) and $W_{LSR} > 0$ (dotted line), showing D_{-} (dashed line) and D_{+} (dot-dashed line).

both the F05 method and the Kuiper symmetry test cannot rule out the presence of these streams in the volume sampled by CORAVEL giants.

The larger volume sampled by the giants than the dwarfs can, however, rule out the presence of the VOD, if their stellar densities estimated from the Fuchs et al. (2006) CADIS fields are realistic. If this is the case, they would consist of 6000-8000 CORAVEL giants, which the Kuiper test can strongly rule out. Table 4 shows that the test can rule out these streams down to a density of $\sim$4000 stars kpc^{-3} (depending on kinematics).

Thick disc and halo stars make up <10 per cent of the sample (high-velocity stars, colour-coded blue in Fig. 10). Therefore, although the CORAVEL giants have extended our search volume to greater vertical distances than the thin disc scaleheight ($\sim$220 pc), it is still dominated by the thin disc. RAVE is the only RV survey that vertically samples significant numbers of thick disc stars (as well as old thin disc stars) at the solar position.

4   RAVE

4.1   RAVE stellar populations

To date (2007 June 26), 220 070 RAVE spectra have been amassed from 196 131 stars. This paper utilizes an internal RAVE data release containing 151 856 RVs, which includes 24 748 RVs from the first public data release[1] (Steinmetz et al. 2006), a similar number of currently unpublished RVs from the forthcoming second public data release (Zwitter et al. 2007, in preparation) and future data releases (see Fig. 11).

Unlike the CORAVEL surveys that targeted specific stellar populations (F-G dwarfs and K-M giants), RAVE does not employ any colour selection or spectral type cuts. This means RAVE observes all the stellar populations within

---

[1] The first public data release of the RAVE catalogue is available and can be retrieved or queried from the RAVE Collaboration website: http://www.rave-survey.org.
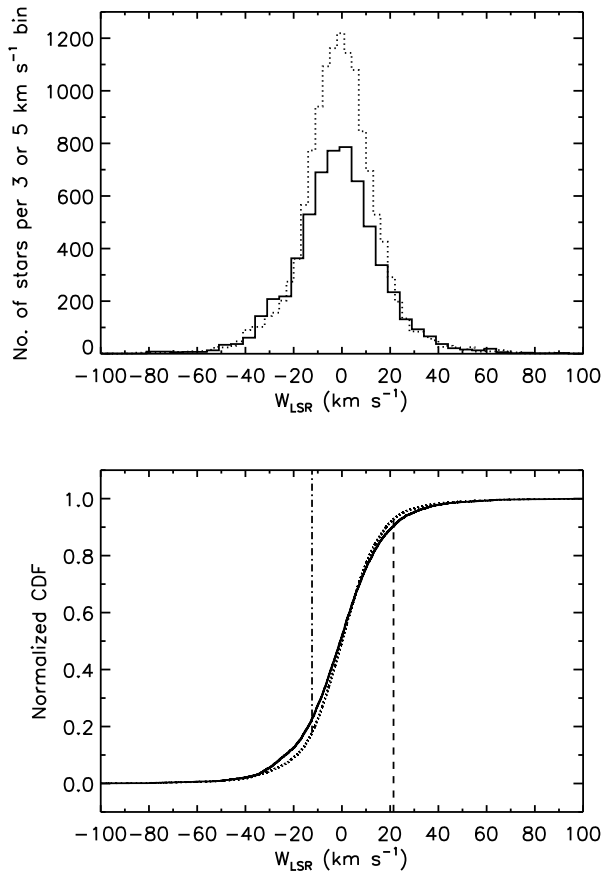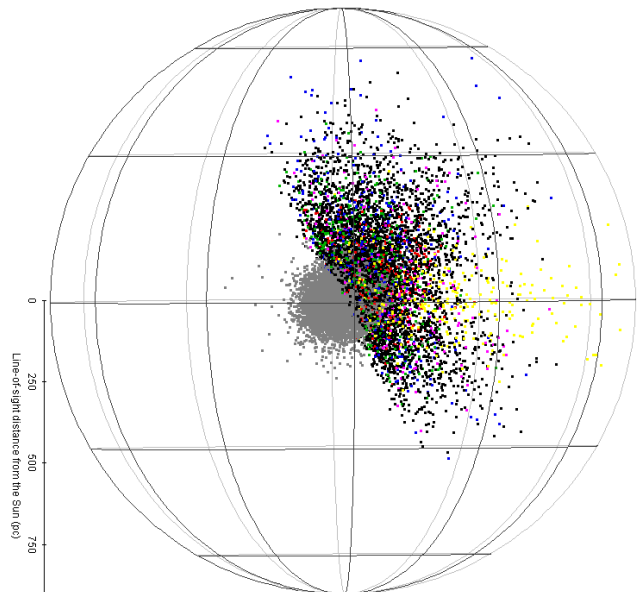
Figure 10. Three dimensional Galactic sky distribution of all the 13 240 CORAVEL dwarfs with W space velocities (grey) and the 6030 CORAVEL giants with W space velocities, including spectroscopic binaries with centre-of-mass RVs, colour-coded the same as in Fig. 6. The spherical polar axes have a radius of 900 pc, centred on the Sun. The viewer's angle is the same as in Fig. 3: chosen to illustrate the 63° between the Earth's equator and the Galactic plane (longest horizontal line), emphasizing that the CORAVEL giants are only visible from the Earth's Northern hemisphere.

Figure 9. *Top:* W_{LSR} distribution of the CORAVEL survey: 6030 giants (solid histogram) and 13 240 dwarfs (dotted histogram). *Bottom:* Normalized CDF of the giants (N_1, solid line) and the dwarfs (N_2, dotted line) as a function of W_{LSR}, where the maximum differences between them are indicated by vertical lines: D_+ (= 0.0509, dot-dashed line) and D_- (= 0.0257, dashed line), where $N_e = 4143.08$, $D = 0.0766$ and $Q = 1 \times 10^{-19}$.

the apparent I magnitude-limited selection functions of its input catalogues (see Fig. 12). Steinmetz et al. (2006) fig. 5 shows that this selection function is much fainter than the CORAVEL (and *Hipparcos*) surveys. Therefore, there is only a few per cent serendipitous overlap of RAVE stars with *Hipparcos* parallaxes (with large errors) and/or Strömgren photometry at the bright end of RAVE. Hence, the distance determination methods described in Section 2.1 are not available to RAVE stars and the method described in Section 3.1 is beyond the scope of this study. RAVE stars cannot be placed in a H-R diagram because sufficiently accurate photometrically derived distances are not yet available (discussed in more detail below).

Instead, we illustrate RAVE's different stellar populations using a reduced proper motion diagram. The concept of reduced proper motion (H) was first used by E. Hertzsprung (Luyten 1968) in the absence of absolute magnitude. Just as parallax fixes the absolute magnitude exactly, H determines the absolute magnitude approximately. When this is plotted against colour, it produces a statistical H-R diagram (kinematic colour-apparent magnitude diagram). H combines the observable properties of proper motion (μ, in

arcsec yr^{-1}) and apparent magnitude [the most comprehensive photometric coverage of observed RAVE stars is the 2MASS Point Source Catalogue (Cutri et al. 2003) so here we choose 2MASS K_S] in the equation

$$H_{K_S} = K_S + 5 \log \mu + 5 = M_{K_S} + 5 \log v_T - 3.379, \quad (13)$$

which also expresses H_{K_S} in terms of the more fundamental properties of absolute magnitude (M_{K_S}) and tangential velocity (v_T in km s^{-1}). Fig. 13 shows that the $H_{K_S}-(J-K_S)$ plane can divide the observed RAVE stars into three distinct stellar populations.

The largest stellar population in the RAVE sample has $J - K_S < 0.5$ mag ($\sim$51 per cent). These stars are mainly thin disc F-G dwarfs [represented on the isochrone by the Main Sequence (MS) at $H_{K_S} = 8$-9 mag]. Although the subgiant branch (represented on the isochrone by the horizontal branch along $H_{K_S} = 6$ mag) is a short phase of stellar evolution (see the Hertzsprung Gap at $J - K_S = 0.5$ mag in Fig. 13), there will be a non-negligible number of subgiants in the RAVE sample. H_{K_S} is unable to kinematically separate the subgiants from the F-G dwarfs because their values of absolute magnitude are too similar for their proper motions to resolve the overlapping kinematics. This results from the overlapping distance ranges of the two populations, due to the large spread in apparent magnitude in Fig. 12.

The two populations with $J - K_S > 0.5$ mag have sufficiently different absolute magnitudes for their proper motions to resolve the very different kinematics resulting from the very different distance ranges of the two populations. The fainter population ($\sim$5 per cent) are thin disc K-M
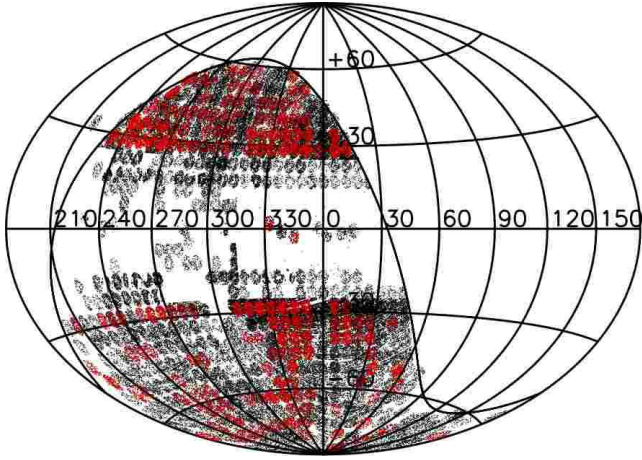
Figure 11. Aitoff projection of the Galactic co-ordinates (in degrees) of the 151 856 RVs in the internal RAVE data release (black dots) and the 24 748 publicly available RVs from the first data release (red dots). The vast majority of RAVE data is below the plotted celestial equatorial plane ($\delta = 0°$). The pattern is due to the survey field centres of the first and second input catalogues being defined on $5.7°$ and $5.0°$ grid spacing respectively (the field of view of the 6dF field plates is $5.7°$).

Figure 13. Reduced proper motion diagram of 149 660 RAVE RVs (2196 either do not have 2MASS photometry or measured proper motions). The solar-scaled Padova 2MASS isochrone (Bonatto et al. 2004, red line), chosen to be representative of thin disc stellar populations (2.5 Gyr old, initial metal fraction = 0.019, [Fe/H] ≈ -0.02 dex), has been given thin disc kinematics ($v_T \approx 30$ km s^{-1} in equation 13) in order to interpret RAVE's stellar populations (approximately partitioned by the dashed lines).

Figure 12. DEep Near-Infra Red Survey (DENIS, Epchtein et al. 1999) *I*-band selection functions of 131 632 RAVE RVs, observed with the two RAVE input catalogues. *Tycho-2* and the SuperCOSMOS Sky Survey (SSS, Hambly et al. 2001) were used to generate the first and second RAVE data releases (see Steinmetz et al. 2006 for details) and contribute 64 581 RVs to the plot (49 per cent). DENIS was used to define the current input catalogue, which is still being observed and will generate all future data releases and contributes 67 051 RVs to the plot (51 per cent). (20 224 RAVE RVs are not included in the plot because of incomplete DENIS sky coverage.)

dwarfs (represented on the isochrone by the MS at H_{K_S} = 9-14 mag). The brighter population ($\sim$44 per cent) are K-M giants (represented on the isochrone by the Red Giant Branch at $H_{K_S} = 1$-4 mag). Although the RAVE giant sample is still dominated by the thin disc, their intrinsic brightnesses probe distances that sample a statistically significant number of thick disc stars and a non-negligible number of inner halo stars.

4.2 Distances to RAVE stars

Fig. 13 shows that H_{K_S} bifurcation can be used to kinematically select K-M dwarfs, without spectroscopically derived $\log g$, to derive photometric distances. Their atmospheres are dominated by saturated molecular bands so their luminosity is not very sensitive to metallicity. This means isochrones for this population are very similar for different metallicities and ages, leading to small photometric distance errors. RAVE K0 dwarfs probe $\sim$50-250 pc from the Sun. This volume has already been sampled by the CORAVEL dwarfs (see Fig. 3) and shown to be devoid of tidal streams in Section 2. Therefore there is no advantage to searching this volume again with RAVE's less accurate W space velocities.

The largest uncertainty in deriving photometric distances to the RAVE F-G dwarfs is stellar age. Absolute magnitude is most sensitive to age close to the MS turnoff. Unlike the CORAVEL dwarfs, RAVE does not have an independent source of trigonometric parallax from which distances can be inferred. This enables stars to be placed in the H-R diagram and allows age to be estimated from a star's evolution away from the zero-age MS. In principle, a chromospheric activity indicator is present in RAVE spectra in the form of Ca II emission. This feature declines with time (as stellar rotation decreases with age) but decays into invisibility at about the age of the Sun. Ranking age using this diagnostic is fraught with systematic errors. RAVE F-G dwarfs probe similar distances ($\sim$200-400 pc) to the CORAVEL giants but are complementary in their non-overlapping sampled volumes (CORAVEL giants are Northern celestial hemisphere only and RAVE is Southern celestial hemisphere only – see Fig. 10). Therefore, there is potential advantage to deriving RAVE F-G dwarf space velocities. However, the associated errors will not yield a reliable W distribution to search for asymmetries.

Absolute magnitude is sensitive to [α/Fe] as well as

[Fe/H]. RAVE K-M giants include thick disc and halo stars, which have, compared to the thin disc, enhanced [α/Fe]. Metallicity uncertainty dominates the uncertainty in deriving photometric distances to the RAVE K-M giants.

Stars in the first RAVE data release were observed without a blue light blocking filter (OG531). Their spectra were contaminated with second order light, which means stellar parameters are not currently available for these stars (see Steinmetz et al. 2006 for details). Stars in all future RAVE data releases have all been observed with an OG531 filter so their spectra only contain first order light. Stellar parameters can be derived for these spectra from the best-match synthetic spectrum. At the time of writing, the accuracy of these parameters is being finalized ready for the second data release (Zwitter et al. 2007, in preparation). The log g is likely to be sufficiently accurate to resolve the $J - K_S > 0.5$ mag sample into dwarfs and giants. However, the log g errors may not be small enough to resolve the $J - K_S < 0.5$ mag sample into dwarfs and subgiants.

RAVE K-M giants probe greater distances ($\sim$0.7-3 kpc) than the CORAVEL giants. Therefore, there is great advantage to deriving the space velocities of RAVE K-M giants because it is unexplored phase space on Galactic scales in between the very local thin disc and inner halo at the solar position. However, tangential velocity errors scale with distance from the Sun. The absolute magnitudes of nearby *Hipparcos* red clump giants show no correlation with [Fe/H]. They have a mean $M_K = -1.61 \pm 0.03$ and $\sigma_{M_K} \approx 0.22$ mag (Alves 2000), which translates to a distance error of $\sim$11 per cent. At 1 kpc, this distance error converts $\Delta\mu = 2$ mas yr^{-1} to $\Delta v_T = 10$ km s^{-1} (Veltz et al. 2007) and ergo $\Delta W > 10$ km s^{-1}. The red clump RAVE giants have the smallest distance error of all the RAVE giants but their values of ΔW are still too large to resolve any dynamically cold, vertical tidal streams falling through the sample. The availability of RAVE giant metallicities would therefore not improve the situation. Outside the red clump, a RAVE K giant at a distance of 1 kpc with proper motion errors at a more typical level of 3.5 mas yr^{-1} and a distance error >15 per cent, due to the uncertainty in [Fe/H], results in $\Delta v_T > 20$ km s^{-1} and ergo $\Delta W > 20$ km s^{-1}.

4.3 RAVE radial velocity determination and accuracy

The RAVE RV pipeline matches each RAVE spectrum with a theoretical spectrum from the Zwitter et al. (2004) and Munari et al. (2005) libraries. These libraries contain thousands of stellar templates, whereas CORAVEL uses only one template. The RAVE RV pipeline uses the standard cross-correlation procedure (Tonry & Davis 1979), implemented in the IRAF package XCSAO (Kurtz et al. 1992), to derive RVs and internal RV errors. Fig. 14 shows the mode of the internal RV error distribution is $\sim$1 km s^{-1}. A RV zero-point error of $\sim$1 km s^{-1} makes the mode of the external RV error distribution $\sim$2 km s^{-1}.

We use the Tonry-Davis cross-correlation coefficient (r, Tonry & Davis 1979) to impose a quality cut. r is a measure of template match to spectra. Excluding RVs with $r < 15$, removes poor-quality spectra and a small number of hot dwarfs due to template-mismatches. This is seen in the proportion of RAVE RVs with $J - K_S < 0.5$ mag and $r > 15$
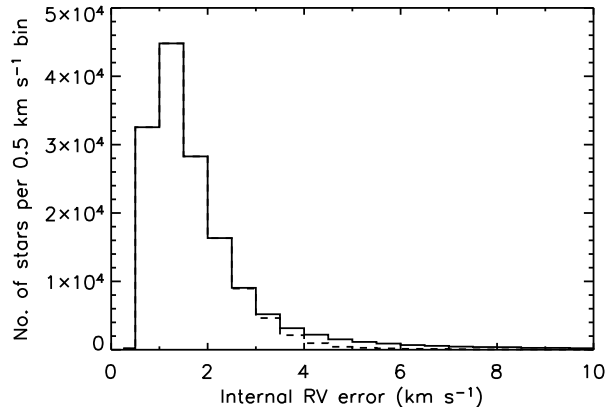

Figure 14. Distribution of internal RV errors for all 151 856 RAVE RVs (all values of r, solid line) and the 140 228 RVs with $r > 15$ (dashed line).

decreasing from $\sim$51 to 50 per cent. Fig. 14 shows this cut decreases the amplitude of the tail of the internal RV error distribution, which has sufficient accuracy to resolve dynamically cold streams.

RAVE RV accuracy compares favourably with the CORAVEL accuracy because the two strongest Calcium triplet absorption lines in the RAVE spectroscopic region (8410-8795 Å) are powerful RV diagnostics at RAVE's medium resolution ($R \sim 7500$). Steinmetz et al. (2006) cross-matched RAVE first data release targets with the CORAVEL dwarfs. Thirteen matches were found but two of them were classified by N04 as binaries. The remaining eleven single targets show good agreement, with a mean difference of 1.4 ± 0.4 km s^{-1} and $\sigma = 1.4$ km s^{-1}.

4.4 RAVE pseudo-W without distances

A star's heliocentric RV cannot be decomposed into the star's constituent U, V and W space velocities because, by definition, RV does not include any tangential contribution. However, a star's RV can be resolved into its line-of-sight (los) components of these space velocities:

$$\mathrm{RV} = \sqrt{(U^{los})^2 + (V^{los})^2 + (W^{los})^2}. \tag{14}$$

We remove the dependence of Galactic latitude on RV by only resolving the components in equation 14 in a single dimension in the Galactic plane,

$$UV^{los} = \sqrt{(U^{los})^2 + (V^{los})^2} = \mathrm{RV} \cos b, \tag{15}$$

and the dimension perpendicular to the Galactic plane,

$$W^{los} = \mathrm{RV} \sin b. \tag{16}$$

The above equations show that for a stellar los along $b = -45°$, RV consists of equal contributions from UV^{los} and W^{los} but for stars with $b < -45°$, as b decreases the contribution of W^{los} to RV increases and RV becomes less and less sensitive to UV^{los}. If a star's los is exactly towards the SGP ($b = -90°$), $W^{los} = W$ because here is there is no tangential component of W. For los with $-90° < b < -45°$, $W^{los} < W$ but W^{los} is a useful proxy for W. Therefore, the issues discussed in the previous section can be circumvented
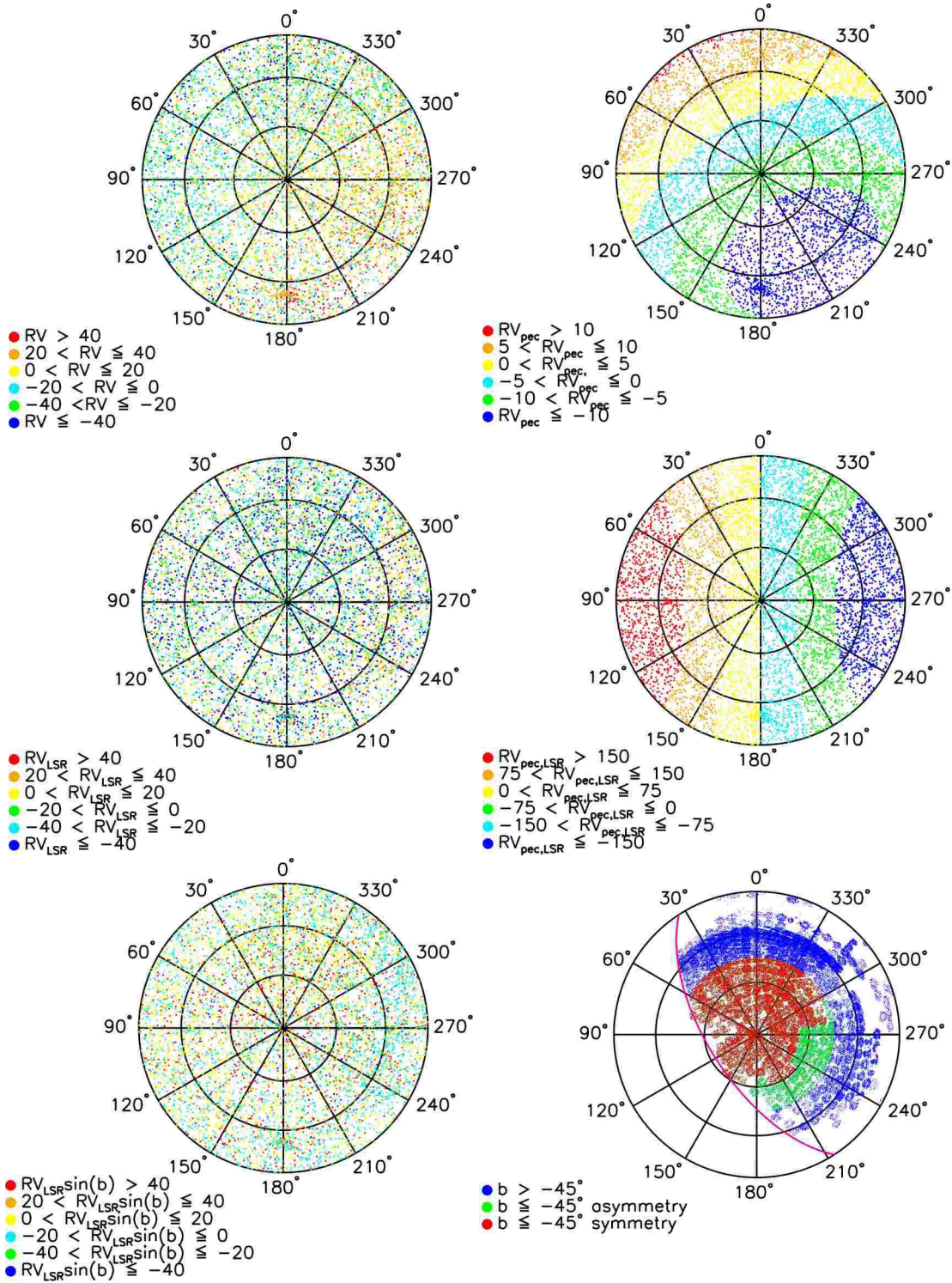
Figure 15. Lambert polar (equal area corresponds to equal solid angle on the sky) projections of the Southern Galactic hemisphere, where the SGP ($b = -90°$) is at the centre and concentric circles correspond to constant b at $-60°$, $-30°$ and $0°$ (Galactic equator), around which the radial lines of constant l are labelled. CORAVEL dwarfs are plotted with their RVs in km s^{-1} colour-coded in different reference frames according to the legend of each plot: heliocentric RV (top left); peculiar RV of the Sun relative to the LSR (solar motion, RV$_{pec}$, top right, see Appendix A for more details); RV with respect to the LSR (RV$_{LSR}$, middle left); peculiar RV of the LSR relative to the GSR (RV$_{pec,GSR}$, middle right); W^{los} (RV$_{LSR} \sin b$, bottom left). The overdensity at $l \sim 180°$, $b \sim -20°$ is the Hyades open cluster. *Bottom right*: RAVE stars colour-coded according to RAVE field symmetry about $l = 180°$. The magenta curve traces the celestial equatorial plane ($\delta = 0°$).

by using the accuracy of the RAVE RVs towards the SGP with $b < -45°$.

The top two plots in Fig. 15 show that for differing los, RV in equation 16 is sensitive to differing amounts of solar motion with respect to the LSR. In order to compare W^{los} along different los in the same reference frame, RV in equation 16 is replaced by RV_{LSR}, which is RV corrected for the solar motion, decomposed into its cardinal directions along the los relative to the LSR:

$$
\begin{aligned}
RV_{LSR} = & \ RV + U^{\odot}_{LSR} \cos l \cos b + V^{\odot}_{LSR} \sin l \cos b \\
& + W^{\odot}_{LSR} \sin b.
\end{aligned}
\tag{17}
$$

The middle left plot in Fig. 15 shows that the LSR reference frame removes the peculiar components of the solar RV (top right plot) from the RV los (top left plot). However, like RV, RV_{LSR} is still dependent on the los. The middle right plot in Fig. 15 shows that RV_{LSR} is sensitive to differing amounts of the peculiar RV of the LSR relative to the GSR,

$$
RV_{pec,GSR} = V_{rot} \sin l \cos b.
\tag{18}
$$

The net Galactic rotation from $l = 270°$ to $l = 90°$ is just visible in the middle left plot of Fig. 15 towards ($l = 90°$) and against ($l = 270°$) the Galactic rotation directions: the $0° < l < 180°$ CORAVEL dwarfs have slightly more stars with $RV_{LSR} < 0$ than $RV_{LSR} > 0$ and vice versa for $180° < l < 360°$ (RV_{LSR} exhibits the pattern in equation 18 and the middle right plot in Fig. 15 because it mirrors RV_{GSR}). Although F05 showed that the presence of dynamical streams causes there to be a net radial motion in the solar neighbourhood (see Appendix A), this is in phase space and independent of l. Thus the U^{los} contribution to RV_{LSR} is isotropic as illustrated by the symmetry in RV_{LSR} between the regions near the cardinal U directions ($l = 0°$ and $l = 180°$) in the middle left plot in Fig. 15.

It is not appropriate to correct RV_{LSR} for Galactic rotation because we are resolving RV_{LSR} perpendicular to the Galactic plane and the correction does not affect W^{los} because $W = 0$ in equation 18. However, because this correction is not applied to RAVE stars towards the SGP ($b < -45°$), the small component of RV_{LSR} sensitive to Galactic rotation (V^{los}) propagates through equation 16. The effect of V^{los} is just visible in the bottom left plot in Fig. 15, where $\sin(b < 0°)$ reverses the sign of the effect i.e. the $0° < l < 180°$ CORAVEL dwarfs have slightly more stars with $W^{los} > 0$ than $W^{los} < 0$ and vice versa for $180° < l < 360°$. A Kuiper symmetry test on the W^{los} distribution of $b < -45°$ CORAVEL dwarfs is similar to the results in Section 2.4 because the W^{los} sample is symmetric about $l = 180°$, so that the positive and negative V^{los} contributions cancel out.

A Kuiper symmetry test on the W^{los}_{LSR} distribution of RAVE stars with $b < -45°$ and $r > 15$ strongly rejects the null hypothesis (that $W^{los}_{LSR} > 0$ and $W^{los}_{LSR} < 0$ are drawn from the same parent population) at $Q \sim 1 \times 10^{-9}$, where $W^{los,\odot}_{LSR} = 4.1$ km s^{-1} to the nearest 0.1 km s^{-1}. The bottom right plot in Fig. 15 shows that, because the RAVE sample is Southern celestial hemisphere only, it does not symmetrically sample the SGP out to $b = -45°$. This plot reveals the largest part of the $b < -45°$ asymmetry at $l > 180°$ (colour-coded green) is not observed by RAVE at $l < 180°$ because it is in the Northern hemisphere. The contribution

of V^{los} to RV_{LSR} in this region of $l > 180°$ cannot cancel with its $l < 180°$ mirrored region so the Kuiper symmetry test finds the difference in the W^{los}_{LSR} distribution.

To rectify this, we only sample $b < -45°$ RAVE fields that are symmetrically positioned either side of $l = 180°$ (28 868 RVs colour-coded red in the bottom right plot of Fig. 15). Because RAVE observes some fields more than once (normally different stars each visit), differing stellar densities are visible in this plot. In the Galactic sky-symmetric sample, there are more $r > 15$ RVs with $l > 180°$ (16 235) than $l < 180°$ (12 633). Nevertheless, the next section shows that the Kuiper symmetry test fails to reject the null hypothesis, showing that our Galactic sky-symmetric sample can be used to search for streams without any further processing. Its selection function is almost identical to Fig. 12, apart from nearly all the $9 < I < 10$ mag stars come from the first input catalogue rather than the second. The stellar population proportions of the subsample are different to the whole RAVE sample. F-G dwarfs have increased most to $\sim$61 per cent, K-M dwarfs have increased to $\sim$7 per cent and K-M giants have decreased to $\sim$32 per cent. The internal RV error distribution of the subsample is the same as the whole sample with $r > 15$.

4.5 Determining RAVE W^{los}_{LSR}

We repeated the Kuiper test in Section 2.3, comparing the $b < -45°$ $RV_{LSR} \sin b$ distribution of all the CORAVEL dwarfs with the single dwarfs and found them to be more similar than the W_{LSR} test ($Q = 0.9998$ but N_e is only 779). This demonstrates that all the RAVE (and SEGUE) RVs can also be used to look for tidal streams without worrying about the affects of binarity. This section repeats the technique applied to the CORAVEL stars in Sections 2.4 and 3.3 to RAVE stars.

The top of Fig. 16 shows the W^{los}_{LSR} distribution for the minimum value of D, where $W^{los,\odot}_{LSR} = 1.7$ km s^{-1} to the nearest 0.1 km s^{-1}. The difference between this value and the $W^{\odot}_{LSR} = 7.0$ km s^{-1} values derived from the CORAVEL dwarfs and giants highlights that $W^{los}_{LSR} \not\equiv W_{LSR}$ but merely a proxy. The D_- and D_+ positions in the bottom plot of Fig. 16 are similar to the CORAVEL positions in Figs 4 and 7, suggesting W^{los}_{LSR} does approximate W_{LSR}. $W^{los,\odot}_{LSR}$ is nearly in agreement with the mode of the W^{los}_{LSR} distribution in Fig. 16. Again, this suggests that there cannot be many stars belonging to vertically coherent streams with systemic W_{LSR} velocities. Table 5 shows that the RAVE N_e value is more than double the value for the CORAVEL samples. The RAVE Q value is double the value for the CORAVEL dwarfs but less than the value for the CORAVEL giants. The RAVE $\Delta W^{los,\odot}_{LSR}$ values are more symmetric than the CORAVEL values.

4.6 Sensitivity of RAVE W^{los}_{LSR} symmetry to tidal streams

To estimate the volume probed by our RAVE sample, we consider that RAVE stars fainter than $I = 12$ mag contribute a negligible number of stars to the sample (see Fig. 12). This sets a distance limit for a typical RAVE giant ($M_I = -0.25$ mag) at $\sim$3 kpc. We approximate the volume of each RAVE

Table 5. Results of the Kuiper symmetry test, applied to our RAVE sample, to determine $W_{LSR}^{los,\odot}$ to the nearest 0.1 km s^{-1}, where $\Delta W_{LSR}^{los,\odot} = W_{LSR}^{los,\odot} - 1.7$ km s^{-1}.

$W_{LSR}^{los,\odot}$	$\Delta W_{LSR}^{los,\odot}$	$N_{W_{LSR}^{los}<0}$	$N_{W_{LSR}^{los}>0}$	N_e	D_-	D_+	D	Q
0.4	−1.3	14 742	14 126	7214	0.0318	0.0005	0.0323	1×10^{-5}
1.7	0.0	14 026	14 842	7211	0.0146	0.0053	0.0199	0.0658
2.7	1.0	13 455	15 413	7184	0.0119	0.0196	0.0315	3×10^{-5}

Table 6. Results of the Kuiper symmetry test, applied to our RAVE sample, to determine the approximate number of tidal stream stars (N_s), required in pseudo-randomly generated $\sigma_s = 10$ km s^{-1} Gaussians, placed at $\pm(1, 2, 3, \sim7)\sigma_{W_{LSR}^{los}}$ in the W_{LSR}^{los} distribution, to cause the test to reject the null hypothesis at 4σ ($Q < 6 \times 10^{-5}$). % = $N_s/(N_s + N_{total})$ where $N_{total} = 28\ 868$. ρ_s is the range of stellar density of each stream, in N stars kpc^{-3}, calculated by dividing the N_s of each stream by our RAVE sample volume (~8 kpc^{-3}, see text for details), modulated by the 5-15 per cent RAVE completeness, which increases ρ_s by a factor of 20-6.7 respectively.

$\sigma_{W_{LSR}^{los}}$	N_s	%	ρ_s	$N_{W_{LSR}^{los}<0}$	$N_{W_{LSR}^{los}>0}$	N_e	D_-	D_+	D	Q
−1	500	1.7	400-1300	14 525	14 843	7341	0.0303	0.0031	0.0334	5×10^{-6}
1	600	2.0	500-1500	14 027	15 441	7350	0.0135	0.0185	0.0320	2×10^{-5}
−2	300	1.0	250-750	14 326	14 842	7290	0.0296	0.0039	0.0335	5×10^{-6}
2	500	1.7	400-1300	14 026	15 342	7327	0.0074	0.0235	0.0309	4×10^{-5}
−3	300	1.0	250-750	14 326	14 842	7290	0.0318	0.0039	0.0357	6×10^{-7}
3	600	2.0	500-1500	14 026	15 442	7350	0.0041	0.0310	0.0351	9×10^{-7}
~-8	300	1.0	250-750	14 326	14 842	7289	0.0319	0.0039	0.0358	5×10^{-7}
~8	500	1.7	400-1300	14 026	15 342	7327	0.0002	0.0321	0.0323	1×10^{-5}

field as a cone of height 3 kpc subtending the RAVE field diameter of 5.7°. Our sample is complicated by the inclusion of stars from two input catalogues with the co-ordinates of its field centres based on grids offset from each other. Fig. 17 shows that the first RAVE input catalogue (colour-coded red) consists of contiguous fields on a 5.7° grid. The second RAVE input catalogue (colour-coded black) is based on a 5.0° grid and so the 5.7° field of view 6dF fields overlap each other, as well as overlapping the fields of the first input catalogue. We have counted the number of contiguous (red) fields in Fig. 17 and estimated, to the nearest half field, the additional sky covered by the non-overlapping parts of the other fields (black). The sample consists of ~113 fields, giving a volume of ~8 kpc^3.

Steinmetz et al. (2006) estimated the RAVE completeness of the old *Tycho-2* and SSS input catalogue in their fig. 4 to be ~15 per cent compared to DENIS at the bright end of the selection function ($I \sim 10$ mag). This drops to ~5 per cent at the faint end ($I \sim 12$ mag). Subtle colour biases exist in the old input catalogue but more than half our sample comes from the unbiased DENIS input catalogue. This should reduce the effect of the biases and increase the completeness levels but we use the old input catalogue levels as a conservative estimate.

This section repeats the technique applied to the CORAVEL stars in Sections 2.5 and 3.4 to the RAVE stars, except the RAVE dispersion is much larger: $\sigma_{W_{LSR}^{los}} \approx 29$ km s^{-1} and thus now $\pm8\sigma_{W_{LSR}^{los}}$ approximately corresponds to the $\pm W_{LSR}^{los}$ values of the H99b streams.

Table 6 shows that the positions of D_- and D_+ appear to cause the $+W_{LSR}^{los}$ distribution to be insensitive to the position of the stream and the number of its members. As before, the test becomes more sensitive (less stream stars

required to generate a 4σ detection), the further a stream is from the centre of the distribution in the $-W_{LSR}^{los}$ distribution. However, Table 6 shows that, again, the number of stream stars required for a 4σ detection stays approximately constant (saturates) at $W_{LSR} \leqslant -3\sigma_{W_{LSR}}$.

Fig. 18 shows that there are a few RAVE stars with similar W_{LSR}^{los} as both the $+W_{LSR}$ ($250 < W_{LSR} < 350$ km s^{-1}) and $-W_{LSR}$ ($-250 < W_{LSR} < -200$ km s^{-1}) H99b streams. Without distances to these stars to check their orbital angular momenta, they cannot be confirmed as members of the H99b streams. Regardless of the symmetry between the two streams, Table 6 shows that there are far too few of these stars for the Kuiper symmetry test to detect them as a stream.

Assuming 5 per cent RAVE completeness, the lower bound of the Freese et al. (2005) estimates of the Sgr stream stellar density predict that ~80 RAVE stars could be Sgr stream stars. This increases to ~590 stars using the upper bound. Assuming a less conservative RAVE completeness level of 15 per cent, predicts between ~250-1780 Sgr stars. The number of VOD stars that could be in RAVE is $\gtrsim48\ 000$. Therefore, the superior volume of RAVE rules out the possibilities that the Sgr stream and VOD cross the Galactic disc through the solar neighbourhood. It also puts much tighter constraints than the CORAVEL surveys on the density of any stream that could be passing through the solar neighbourhood, ruling out any streams with similar densities to the Sgr stream.
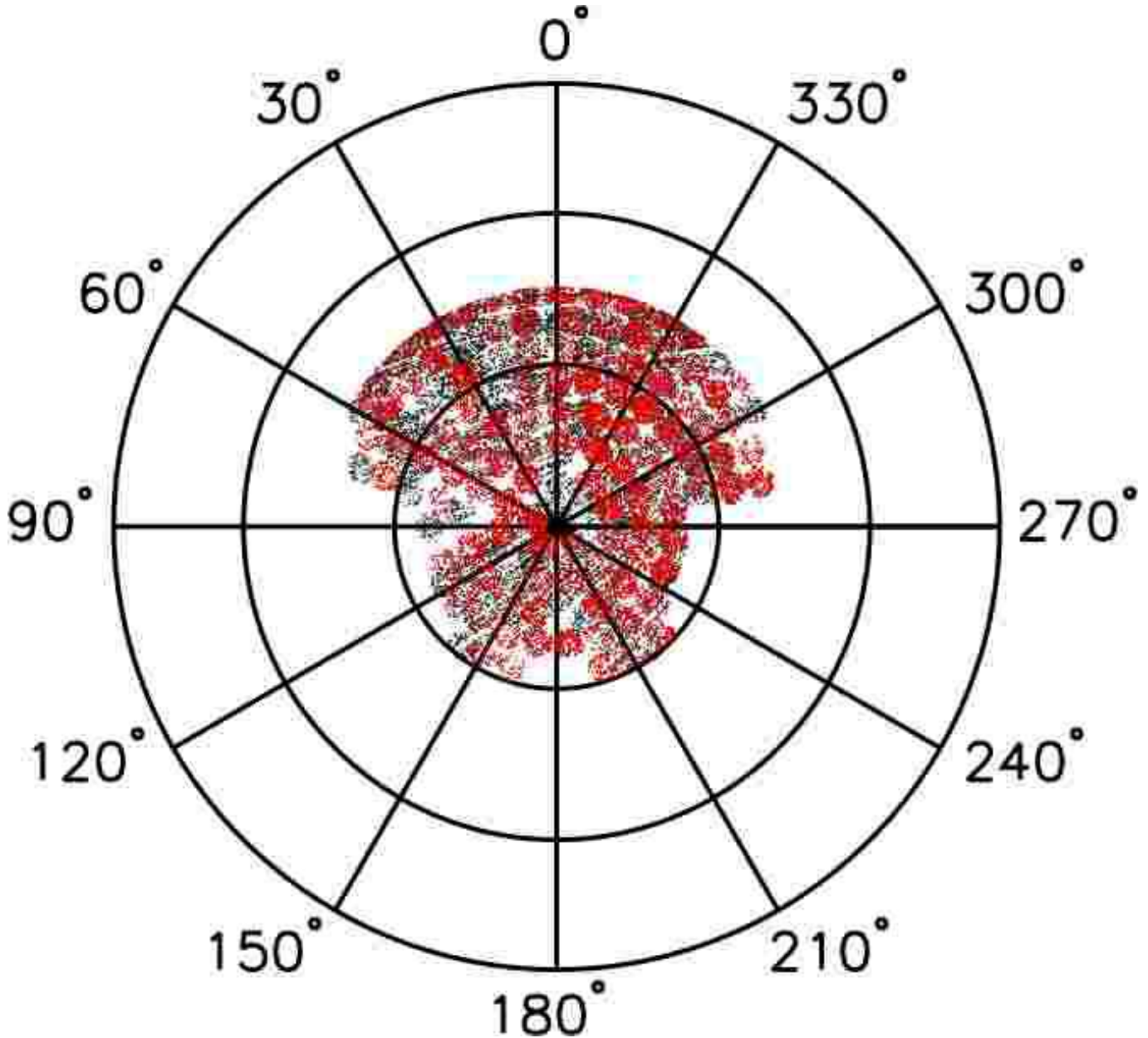
Figure 17. Same as the bottom right plot of Fig. 15 except only the Galactic sky-symmetric RAVE sample is plotted and is colour-coded according to input catalogue: 5.7° grid spacing (red) and 5.0° grid spacing (black). The blank strips (aligned with the declination axis) in between the black dots are due to the incomplete sky coverage of DENIS data.

4.7 Comparing RAVE and CORAVEL $W_{LSR}^{(los)}$ and sampled volumes

Table 7 presents the Kuiper test results from comparing the entire RAVE W_{LSR}^{los} distribution with the entire CORAVEL dwarfs (Fig. 19) and giants W_{LSR} distributions (Fig. 20). The test finds the largest differences at $\sim\pm 1\sigma_{W_{LSR}}$ in the CORAVEL distributions because of the greater RAVE $\sigma_{W_{LSR}^{los}}$, due to the larger volume it samples. A comparison of the respective volumes sampled by the surveys is depicted in Fig. 21. It shows that only the $\sim$2000 RAVE K-M dwarfs probe the same volume as the CORAVEL F-G dwarfs. The $\sim$17 600 RAVE F-G dwarfs fill in the SGP at $b < -45°$ not probed by the CORAVEL giants. It is the $\sim$9200 RAVE

giants that really extends our tidal stream search into the thick disc, its scaleheight being $\sim$1 kpc (Veltz et al. 2007). Because of the differing distance ranges covered by the different RAVE stellar populations, we have repeated our search procedure on each population separately (as defined in Fig. 13). This has been investigated in case e.g. the asymmetry of a thick disc or halo stream of giants is smeared out by the more numerous sample of dwarfs. However, a Kuiper symmetry test on each component fails to reject the null hypothesis. F-G dwarfs are found to be the most symmetric, then K-M dwarfs with the K-M giants the least symmetric.
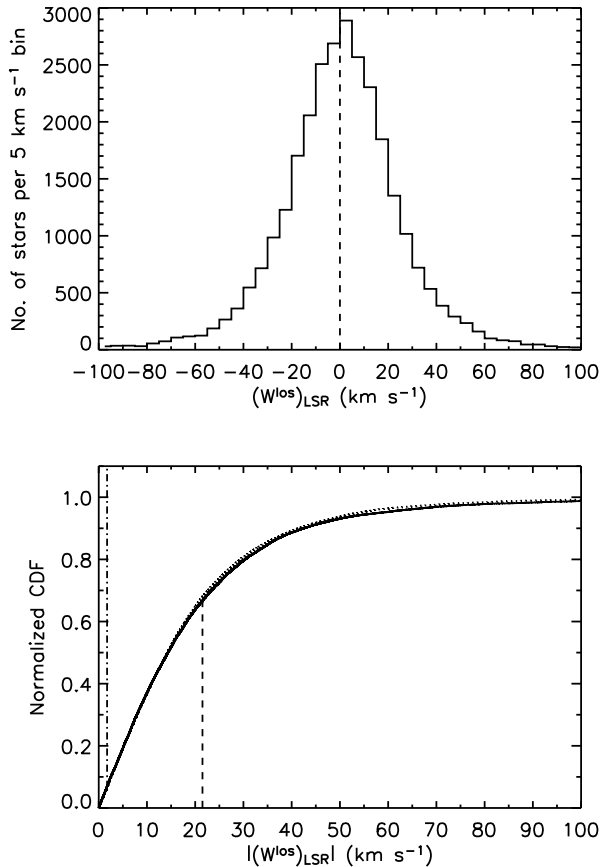
Figure 16. *Top:* W_{LSR}^{los} distribution of RAVE stars with $b < -45°$ (solid histogram) either side of the $W_{LSR}^{los} = 0$ dividing line (dashed lines). The 5 km s^{-1} velocity bin sizes are chosen to be more than twice the mode of the RAVE external RV error ($\sim$2 km s^{-1}). *Bottom:* Normalized CDF of $W_{LSR}^{los} < 0$ (solid lines) and $W_{LSR}^{los} > 0$ (dotted lines), showing D_- (dashed lines) and D_+ (dot-dashed lines).

Table 7. Kuiper test results comparing the RAVE W_{LSR}^{los} distribution to the CORAVEL dwarfs and giants W_{LSR} distributions.

CORAVEL	N_e	D_-	D_+	D	Q
Dwarfs	9077	0.1060	0.0974	0.2034	$<10^{-37}$
Giants	4988	0.0863	0.0538	0.1401	$<10^{-37}$

5   DISCUSSION

We have searched the CORAVEL and RAVE surveys for evidence of a net vertical flow through the solar neighbourhood that could be associated with a tidal stream of stars with vertically coherent kinematics. Due to the current unavailability of accurate distances to RAVE stars, we have used the Kuiper statistic to test the symmetry of the vertical velocity distribution function of the samples. In particular, the test serves as a useful first search for the presence of prominent, kinematically coherent, vertical tidal streams in the RAVE data, which probes further into thick disc and inner halo phase space than any other survey of the local Galactic volume. Using the Geneva-Copenhagen stellar binarity flag,
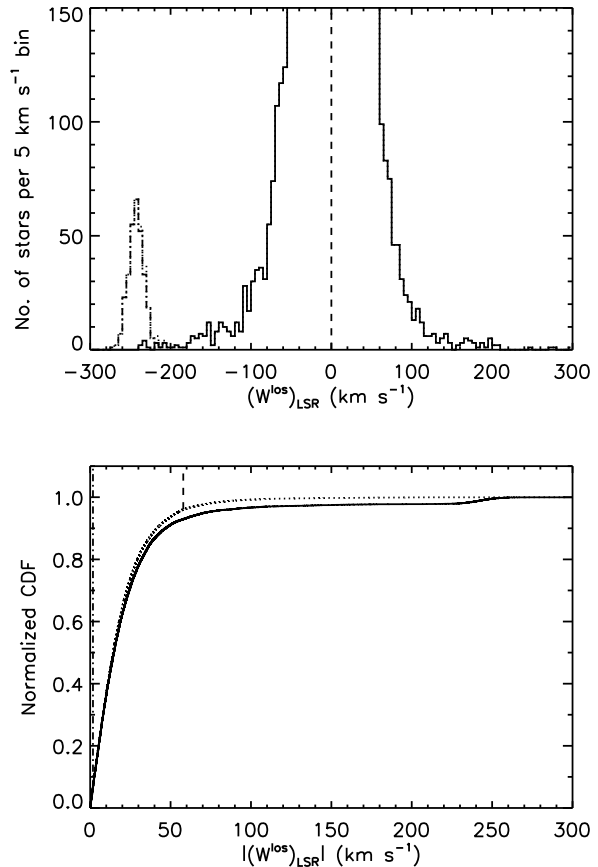
Figure 18. *Top:* RAVE W_{LSR}^{los} distribution (solid histogram) either side of the $W_{LSR} = 0$ dividing line (dashed line). The randomly-generated Gaussian (representing a $\sigma = 10$ km s^{-1} tidal stream) included in the data set (dotted histogram) that cause the Kuiper symmetry test to reject the null hypothesis at 4σ when placed at $\sim-8\sigma_{W_{LSR}}$ is also plotted separately (dot-dashed line). *Bottom:* Normalized CDF of $W_{LSR}^{los} < 0$ (solid line) and $W_{LSR}^{los} > 0$ (dotted line), showing D_- (dashed line) and D_+ (dot-dashed line, just visible at $|W_{LSR}^{los}| \approx 0$).

we demonstrate that binarity has a statistically insignificant effect on the W and $RV_{LSR} \sin b$ velocity distribution functions of the CORAVEL dwarfs, allowing us to use all the CORAVEL dwarfs and RAVE radial velocities (RVs) in our search.

A tidal stream falling slowly through the solar neighbourhood volumes considered (see Table 5) needs to be very coherent for our Kuiper symmetry test to detect it against the background $W_{LSR}^{(los)}$ distribution at $|W_{LSR}^{(los)}| \lesssim \sigma_{W_{LSR}^{(los)}}$. As expected, there is a general trend that the test can detect smaller numbers of stars in a coherent stream the further from the centre of the distribution the stream is, out to $\sim\pm3\sigma_{W_{LSR}^{(los)}}$. However, further into the tails of the distribution the test becomes insensitive to the position of the stream and it is the number of stream members that cause the $+W_{LSR}^{(los)}$ and $-W_{LSR}^{(los)}$ CDFs to diverge sufficiently to generate a stream detection. This number appears to approximately saturate at $|W_{LSR}^{(los)}| \gtrsim 3\sigma_{W_{LSR}^{(los)}}$ and is set by the detection threshold at $\sim\pm3\sigma_{W_{LSR}^{(los)}}$. The required number of
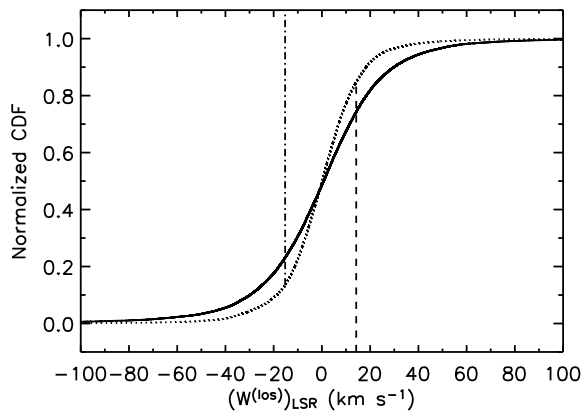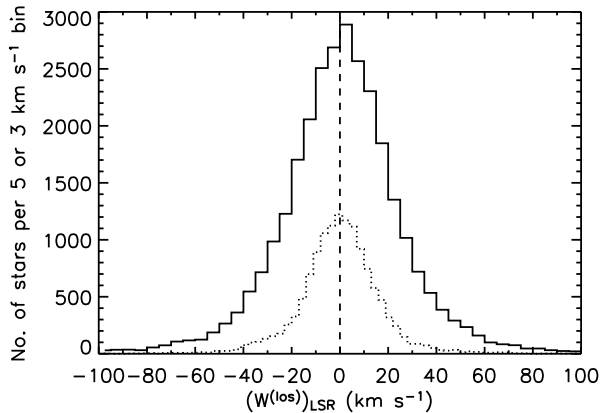
Figure 19. *Top:* $W_{LSR}^{(los)}$ distribution of the 28 868 RAVE stars (solid histogram) and the 13 240 CORAVEL dwarfs (dotted histogram). *Bottom:* Normalized CDF of RAVE (solid line) and CORAVEL dwarfs (dotted line) as a function of $W_{LSR}^{(los)}$, where the maximum differences between them are indicated by vertical lines: D_+ (dot-dashed line) and D_- (dashed line).
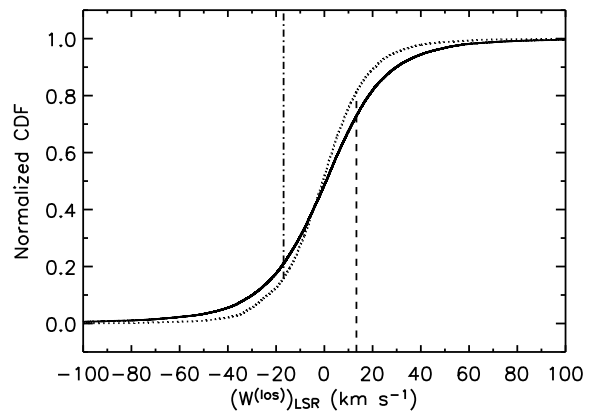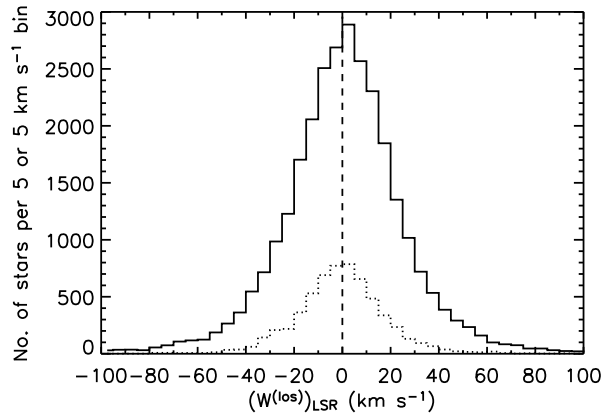
Figure 20. *Top:* $W_{LSR}^{(los)}$ distribution of the 28 868 RAVE stars (solid histogram) and the 6030 CORAVEL giants (dotted histogram). *Bottom:* Normalized CDF of RAVE (solid line) and CORAVEL giants (dotted line) as a function of $W_{LSR}^{(los)}$, where the maximum differences between them are indicated by vertical lines: D_+ (dot-dashed line) and D_- (dashed line).

stars is $\gtrsim 200$. Fig. 18 shows streams should be detectable by eye in the extreme tails of a distribution where more specialized statistical analysis could be applied to test their significance. We have not found any asymmetries in any of our samples that warrant such treatment. Table 8 summarizes the limits we have been able to place on the properties of streams in the solar neighbourhood.

In contrast to the 'Field of Streams' found in the outer halo (Belokurov et al. 2006), we find that the volume of the solar neighbourhood sampled by the CORAVEL and RAVE surveys is devoid of any tidal streams with coherent vertical kinematics containing hundreds of stars. This suggests the Sagitarrius (Sgr) tidal stream does not pass through the solar neighbourhood, which agrees with the latest empirical determination of its orbit (Newberg et al. 2007) and dissociates it from the Helmi et al. (1999) stream (Freese et al. 2004).

The absence of the Sgr stream near the Sun is consistent with simulations of the disruption of Sgr in nearly spherical and prolate Galactic potentials (Helmi 2004; Law et al. 2005; Fellhauer et al. 2006; Martínez-Delgado et al. 2007) and seemingly inconsistent with oblate potentials

(Law et al. 2005; Martínez-Delgado et al. 2007). The constraints on the number of the Sgr stream stars in the solar neighbourhood volume searched in our samples could prove a useful tool for discriminating between Galactic potential models.

The CORAVEL Kuiper symmetry test results are supported by the lack of strong clumping in orbital angular momenta space. The limited range of the CORAVEL giants in angular momenta space shows the Majewski (1992) and Helmi et al. (1999), hereafter H99b, streams are not present in this sample. One of the CORAVEL dwarfs is a member of one of the H99b streams. There is another CORAVEL dwarf with angular momenta and metallicity consistent with the H99b streams. However, we consider it to be a possible outlier because its kinetic energy is too large to be consistent with the energies of the other members of the H99b streams.

The lack of a net vertical flow through the solar neighbourhood argues against the Virgo overdensity (VOD) crossing the disc near the Sun. This agrees with Juric et al. (2005) not finding it within a few kpc of the Sun. Their preliminary analysis of 2MASS M giants did not reveal a similarly large density enhancement to the VOD in the Southern Galactic
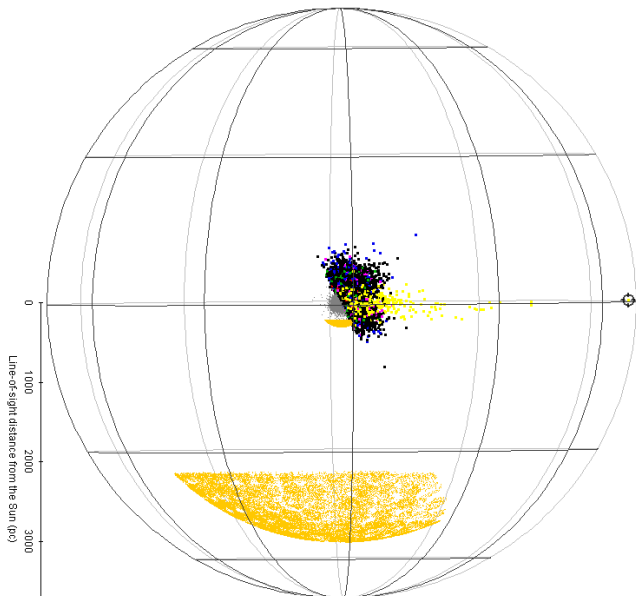
Line-of-sight distance from the Sun (pc) — 0, 1000, 2000, 3000

Figure 21. Three dimensional Galactic sky distribution of all the 13 092 CORAVEL giants with W space velocities (grey), the 6030 CORAVEL giants with W space velocities, including spectroscopic binaries with centre-of-mass RVs, colour-coded according to their maximum likelihood base group assignment in Fig. 6, and the south Galactic cap RAVE sample (orange), where each RAVE star has been assigned a distance of 300 pc, which partitions the maximum distance range of RAVE K-M dwarfs and the minimum distance range of RAVE F-G dwarfs, and a distance of 3 kpc to represent the maximum distance range of $I = 12$ mag RAVE K-M giants. The spherical polar axes have a radius of 3.7 kpc, centred on the Sun, chosen to include the most distant CORAVEL giant with a W velocity (3.6 kpc, marked by the black cursor) with the same viewer's angle as in Fig. 10.

hemisphere. All this evidence is in accord with dark matter being smoothly distributed in configuration space throughout the solar neighbourhood.

Comparison between the volume covered by SDSS photometry in the top right plot of Juric et al. (2005) fig. 20 and the local volume with measured phase space in Fig. 21 highlights the disparity between the two. Juric et al. (2005) extrapolate the four thin and thick disc overdensities seen in their survey volume to the full Galactic disc ($|Z| < 3$ kpc, $R < 15$ kpc) to imply that there are ∼20-40 substructures of this type in the Galaxy, which could be the "missing satellites". It is not too surprising that none of these are within the small Galactic volumes searched in this paper.

Depending on the availability and accuracy of metallicities in the second RAVE data release (Zwitter et al. 2007, in preparation), distances to RAVE giants may be sufficiently accurate to allow action-angle space or integrals of motion space to be searched in the future for clustering indicative of tidal streams. Additional photometric data in the future (e.g. from SkyMapper, Keller et al. 2007) will further reduce distance errors to RAVE stars. However, as in this study, accurate metallicity-derived distances are not required if using RAVE stars towards the cardinal Galactic directions. In the rotation direction ($l \sim 270°$), RVs are dominated by V_{GSR}, where the conversion between the two is only weakly dependent on distance (Woolley 1978; Frenk & White 1980).

Table 8. Summary of how many stream stars (N_s) and their density (ρ_s in N stars kpc^{-3}) are needed for the Kuiper symmetry test to detect them and how many stars (N) from the Sagitarrius stream (Sgr) and Virgo overdensity (VOD) are expected in our sample volumes (V), where the CORAVEL values correspond to the volumes within which they are complete and the RAVE volume is its total approximate volume (its volume completeness (VC) is taken into account). Whether the Kuiper symmetry test is sensitive to the presence of each stream, given their non-local stellar density estimates in the literature is indicated: yes (y), no (n), maybe (?).

Sample	CORAVEL		RAVE	
	Dwarfs	Giants		
Section	2.5	3.4	4.6	
V (kpc^3)	0.0003	0.0511	7.9052	
N_s (low)	200	200	300	
N_s (high)	600	800	600	
VC (%)	100	100	5	15
ρ_s (low)	0.7×10^6	4000	800	300
ρ_s (high)	2.2×10^6	16 000	1500	500
N Sgr (low)	0.1 (n)	10 (n)	80 (n)	250 (?)
N Sgr (high)	0.4 (n)	80 (n)	590 (y)	1800 (y)
N VOD	30 (n)	6000 (y)	48 000 (y)	144 000 (y)

Since J_Z is conserved during phase-mixing, tidal streams should have similar V_{GSR}. Gilmore et al. (2002) found a tidal stream with coherent V_{GSR} in between canonical thick disc and inner halo values. The magnitude range of RAVE was chosen so that its giants probe the interface of the thin and thick discs and inner halo. Hence, RAVE giants can be also used to investigate the angular momenta of the Milky Way's stellar components and its intervening stream(s?) (Seabroke et al. 2007, in preparation).

REFERENCES

Abadi M. G., Navarro J. F., Steinmetz M., Eke V. R., 2003, ApJ, 597, 21

Alves D. R., 2000, ApJ, 539, 732

Baranne A., Mayor M., Poncet J. L., 1979, Vistas in Astronomy, 23, 279

Beers T. C., Chiba M., Yoshii Y., Platais I., Hanson R. B., Fuchs B., Rossi S., 2000, AJ, 119, 2866

Beers T. C., Rossi S., Norris J. E., Ryan S. G., Shefler T., 1999, AJ, 117, 981

Beers T. C., Sommer-Larsen J., 1995, ApJS, 96, 175

Bell E. F., Zucker D. B., Belokurov V., Sharma S., Johnston K. V., Bullock J. S., Hogg D. W., Jahnke K., de Jong J. T. A., Beers T. C., Evans N. W., Grebel E. K., Ivezic Z., Koposov S. E., Rix H.-W., Schneider D. P., Steinmetz M., Zolotov A., 2007, ArXiv e-prints, 706

Belokurov et al. V., 2006, ApJ, 642, L137

Belokurov et al. V., 2007, ApJ, 658, 337

Benson A. J., Frenk C. S., Lacey C. G., Baugh C. M., Cole S., 2002, MNRAS, 333, 177

Bonatto C., Bica E., Girardi L., 2004, A&A, 415, 571

Brown A. G. A., Arenou F., van Leeuwen F., Lindegren L., Luri X., 1997, in Hipparcos - Venice '97 Vol. 402 of ESA Special Publication, Considerations in Making Full Use of the HIPPARCOS Catalogue. pp 63–68

Chiba M., Beers T. C., 2000, AJ, 119, 2843

Chiba M., Yoshii Y., 1998, AJ, 115, 168

Crawford D. L., 1975, AJ, 80, 955

Cutri et al. R. M., 2003, 2MASS All Sky Catalog of point sources.. The IRSA 2MASS All-Sky Point Source Catalog, NASA/IPAC Infrared Science Archive. http://irsa.ipac.caltech.edu/applications/Gator/

De Simone R., Wu X., Tremaine S., 2004, MNRAS, 350, 627

Dehnen W., Binney J. J., 1998, MNRAS, 298, 387

Duffau S., Zinn R., Vivas A. K., Carraro G., Méndez R. A., Winnick R., Gallart C., 2006, ApJ, 636, L97

Epchtein et al. N., 1999, A&A, 349, 236

ESA 1997, The Hipparcos Catalogue, ESA SP-1200

Famaey B., Jorissen A., Luri X., Mayor M., Udry S., Dejonghe H., Turon C., 2005, A&A, 430, 165

Fellhauer M., Belokurov V., Evans N. W., Wilkinson M. I., Zucker D. B., Gilmore G., Irwin M. J., Bramich D. M., Vidrih S., Wyse R. F. G., Beers T. C., Brinkmann J., 2006, ApJ, 651, 167

Fellhauer M., Evans N. W., Belokurov V., Zucker D. B., Yanny B., Wilkinson M. I., Gilmore G., Irwin M. J., Bramich D. M., Vidrih S., Hewett P., Beers T., 2007a, MNRAS, 375, 1171

Fellhauer M., Evans N. W., Belokurov V., Zucker D. B., Yanny B., Wilkinson M. I., Gilmore G., Irwin M. J., Bramich D. M., Vidrih S., Hewett P., Beers T., 2007b, MNRAS, 375, 1171

Freese K., Gondolo P., Newberg H. J., 2005, Phys. Rev. D, 71, 043516

Freese K., Gondolo P., Newberg H. J., Lewis M., 2004, Physical Review Letters, 92, 111301

Frenk C. S., White S. D. M., 1980, MNRAS, 193, 295

Fuchs B., Phleps S., Meisenheimer K., 2006, A&A, 457, 541

Gilmore G., Wyse R. F. G., Norris J. E., 2002, ApJ, 574, L39

Gould A., 2003, ApJ, 592, L63

Grillmair C. J., 2006, ApJ, 645, L37

Hambly N. C., MacGillivray H. T., Read M. A., Tritton S. B., Thomson E. B., Kelly B. D., Morgan D. H., Smith R. E., Driver S. P., Williamson J., Parker Q. A., Hawkins M. R. S., Williams P. M., Lawrence A., 2001, MNRAS, 326, 1279

Helmi A., 2004, ApJ, 610, L97

Helmi A., Navarro J. F., Nordström B., Holmberg J., Abadi M. G., Steinmetz M., 2006, MNRAS, 365, 1309

Helmi A., White S. D. M., 1999, MNRAS, 307, 495

Helmi A., White S. D. M., de Zeeuw P. T., Zhao H., 1999, Nature, 402, 53

Høg E., Fabricius C., Makarov V. V., Urban S., Corbin T., Wycoff G., Bastian U., Schwekendiek P., Wicenec A., 2000, A&A, 355, L27

Holmberg J., Nordstrom B., Andersen J., 2007, ArXiv e-prints, 707

Homann H., 1886, Astronomische Nachrichten, 114, 25

Ibata R. A., Gilmore G., Irwin M. J., 1994, Nature, 370, 194

Johnston K. V., Spergel D. N., Haydn C., 2002, ApJ, 570, 656

Johnston K. V., Zhao H., Spergel D. N., Hernquist L., 1999, ApJ, 512, L109

Juric et al. M., 2005, ArXiv Astrophysics e-prints

Keller S. C., Schmidt B. P., Bessell M. S., Conroy P. G., Francis P., Granlund A., Kowald E., Oates A. P., Martin-Jones T., Preston T., Tisserand P., Vaccarella A., Waterson M. F., 2007, Publications of the Astronomical Society of Australia, 24, 1

Kepley A. A., Morrison H. L., Helmi A., Kinman T. D., Van Duyne J., Martin J. C., Harding P., Norris J. E., Freeman K. C., 2007, AJ, 134, 1579

Kerr F. J., Lynden-Bell D., 1986, MNRAS, 221, 1023

Kinman T. D., Cacciari C., Bragaglia A., Buzzoni A., Spagna A., 2007, MNRAS, 375, 1381

Klypin A., Kravtsov A. V., Valenzuela O., Prada F., 1999, ApJ, 522, 82

Kurtz M. J., Mink D. J., Wyatt W. F., Fabricant D. G., Torres G., Kriss G. A., Tonry J. L., 1992, in Worrall D. M., Biemesderfer C., Barnes J., eds, ASP Conf. Ser. 25: Astronomical Data Analysis Software and Systems I XCSAO: A Radial Velocity Package for the IRAF Environment. pp 432–+

Law D. R., Johnston K. V., Majewski S. R., 2005, ApJ,

619, 807

Luri X., Mennessier M. O., Torra J., Figueras F., 1996, A&AS, 117, 405

Luyten W. J., 1968, MNRAS, 139, 221

Majewski S. R., 1992, ApJS, 78, 87

Majewski S. R., Kunkel W. E., Law D. R., Patterson R. J., Polak A. A., Rocha-Pinto H. J., Crane J. D., Frinchaboy P. M., Hummels C. B., Johnston K. V., Rhee J., Skrutskie M. F., Weinberg M., 2004, AJ, 128, 245

Majewski S. R., Munn J. A., Hawley S. L., 1994, ApJ, 427, L37

Majewski S. R., Munn J. A., Hawley S. L., 1996, ApJ, 459, L73+

Majewski S. R., Skrutskie M. F., Weinberg M. D., Ostheimer J. C., 2003, ApJ, 599, 1082

Martínez-Delgado D., Peñarrubia J., Jurić M., Alfaro E. J., Ivezić Z., 2007, ApJ, 660, 1264

Mayor M., 1985, in Philip A. G. D., Latham D. W., eds, IAU Colloq. 88: Stellar Radial Velocities Cross-Correlation Spectroscopy Using CORAVEL. pp 21–+

Monaco L., Bellazzini M., Bonifacio P., Buzzoni A., Ferraro F. R., Marconi G., Sbordone L., Zaggia S., 2007, A&A, 464, 201

Moore B., Ghigna S., Governato F., Lake G., Quinn T., Stadel J., Tozzi P., 1999, ApJ, 524, L19

Munari U., Sordo R., Castelli F., Zwitter T., 2005, A&A, 442, 1127

Murali C., Dubinski J., 1999, AJ, 118, 911

Newberg H. J., Yanny B., Cole N., Beers T. C., Re Fiorentin P., Schneider D. P., Wilhelm R., 2007, ArXiv e-prints, 706

Newberg H. J., Yanny B., Rockosi C., Grebel E. K., Rix H.-W., Brinkmann J., Csabai I., Hennessy G., Hindsley R. B., Ibata R., Ivezić Z., Lamb D., Nash E. T., Odenkirchen M., Rave H. A., Schneider D. P., Smith J. A., Stolte A., York D. G., 2002, ApJ, 569, 245

Nordström B., Mayor M., Andersen J., Holmberg J., Pont F., Jørgensen B. R., Olsen E. H., Udry S., Mowlavi N., 2004, A&A, 418, 989

Olsen E. H., 1983, A&AS, 54, 55

Olsen E. H., 1984, A&AS, 57, 443

Olsen E. H., 1993, A&AS, 102, 89

Olsen E. H., 1994a, A&AS, 104, 429

Olsen E. H., 1994b, A&AS, 106, 257

Peñarrubia J., Martínez-Delgado D., Rix H. W., Gómez-Flechoso M. A., Munn J., Newberg H., Bell E. F., Yanny B., Zucker D., Grebel E. K., 2005, ApJ, 626, 128

Press W. H., Teukolsky S. A., Vetterling W. T., Flannery B. P., 1992, Numerical recipes in FORTRAN. The art of scientific computing. Cambridge: University Press, —c1992, 2nd ed.

Seabroke G. M., 1879, MNRAS, 39, 450

Seabroke G. M., 1887a, MNRAS, 47, 93

Seabroke G. M., 1887b, Spectroscopic observations of the motion of stars in the line of sight, made at the Temple observatory, Rugby. [London, Spottiswoode & co., printers, 1887]

Seabroke G. M., 1889, MNRAS, 50, 72

Seabroke G. M., Gilmore G., 2007, MNRAS, pp 762–+

Skuljan J., Hearnshaw J. B., Cottrell P. L., 1999, MNRAS, 308, 731

Smith et al. M. C., 2007, MNRAS, 379, 755

Steinmetz et al. M., 2006, AJ, 132, 1645

Tonry J., Davis M., 1979, AJ, 84, 1511

Udry S., Mayor M., Andersen J., Crifo F., Grenon M., Imbert M., Lindegren H., Maurice E., Nordstroem B., Pernier B., Prevot L., Traversa G., Turon C., 1997, in ESA SP-402: Hipparcos - Venice '97 CORAVEL Radial Velocity Surveys of Late-Type Stars of the HIPPARCOS Mission. pp 693–698

Veltz L. et al., 2007, A&A, submitted

Vogel H., 1873, Astronomische Nachrichten, 82, 291

Wilson O. C., 1941, ApJ, 93, 29

Woolley R., 1978, MNRAS, 184, 311

Zacharias N., Urban S. E., Zacharias M. I., Wycoff G. L., Hall D. M., Monet D. G., Rafferty T. J., 2004, AJ, 127, 3043

Zucker et al. D. B., 2006, ApJ, 650, L41

Zwitter T., Castelli F., Munari U., 2004, A&A, 417, 1055

APPENDIX A: HISTORICAL PARALLELS

Soon after Vogel (1873)[2] measured the first reliable RVs of Sirus and Procyon, Seabroke (1879)[3] performed one of the first RV surveys, measuring 68 RVs for 29 stars, followed by 699 RVs for 40 stars (Seabroke 1887a,b) and 866 RVs for 49 stars (Seabroke 1889). Although these visually determined RVs were individually inaccurate, when analysed statistically they showed that the Sun was moving relative to nearby stars at 24.5 ± 15.8 km s^{-1} (Homann 1886). Within the (admittedly large) error, this measurement of solar speed with respect to the LSR agrees with the standard modern measurement of 13.38 ± 0.12 km s^{-1} (calculated from the Dehnen & Binney (1998) solar space velocities in Table A1). Fig. A1 shows the direction of the (Homann 1886) solar apex towards $l = 44.1°$, $b = 8.5°$ is approximately in the same direction as the Dehnen & Binney (1998) values: $l = 27.72°$, $b = 32.43°$.

We have resolved the Homann (1886) solar motion into its Galactic cardinal direction vectors, $U^{\odot}_{LSR}$, $V^{\odot}_{LSR}$ and $W^{\odot}_{LSR}$, assuming the solar apex direction is error-free. It almost certainly is not but Homann (1886) does not quote a directional error so the solar space velocity errors in Table A1 should be considered a lower limit. The Homann (1886) $U^{\odot}_{LSR}$ agrees with more modern estimates within the errors while $V^{\odot}_{LSR}$ and $W^{\odot}_{LSR}$ are close to agreeing within the errors.

Over a century after the Homann (1886) derivation of the solar motion, the debate on this subject in the literature has been revived by the CORAVEL surveys. F05 interpreted the solar neighbourhood substructure in the U-V plane found in their sample of CORAVEL giants and in CORAVEL dwarfs by N04 (and in *Hipparcos* π, μ and RVs by Skuljan et al. 1999) as dynamical streams. Table A1 shows that when F05 excluded all the dynamical streams, they found a different $U^{\odot}_{LSR}$ from when they included all the CORAVEL giants, which agrees with the Dehnen & Binney (1998) value. This discrepancy raises the question of how to

---

[2] A predecessor as director of Potsdam Observatory to MS, co-author of this paper and PI of the RAVE project.
[3] The great-great-grandfather of GMS, first author of this paper.

Table A1. Comparison of the Homann (1886) solar space velocity components compared to more modern estimates.

Author(s)	Data used	$U^{\odot}_{LSR}$ (km s^{-1})	$V^{\odot}_{LSR}$ (km s^{-1})	$W^{\odot}_{LSR}$ (km s^{-1})
Homann (1886)	Seabroke (1879) RVs	17.4 ± 11.2	16.9 ± 10.9	3.6 ± 2.3
Dehnen & Binney (1998)	*Hipparcos* π & μ	10.00 ± 0.36	5.25 ± 0.62	7.17 ± 0.38
This paper	CORAVEL dwarfs			7.0
This paper	CORAVEL giants			7.0
F05	CORAVEL giants	10.25 ± 0.15		7.98 ± 0.09
	Excluding streams	2.78 ± 1.07		8.26 ± 0.38
Veltz et al. (2007)	RAVE RVs, UCAC2^a μ	8.5 ± 0.3		11.1 ± 1.0

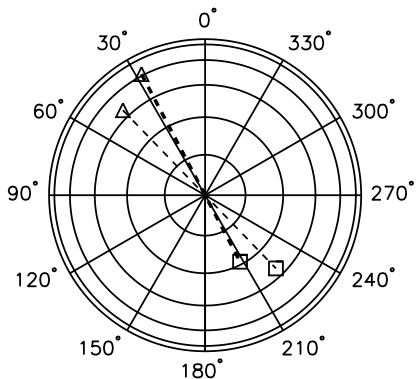^{a} UCAC2 is the Second US Naval Observatory CCD Astrograph Catalogue (Zacharias et al. 2004)

Figure A1. Lambert polar (equal area corresponds to equal solid angle on the sky) projections of the entire Galactic sky, where the SGP ($b = -90°$) is at the centre and concentric circles correspond to constant b at every $30°$ to the outermost circle at $+90°$ (NGP), around which the radial lines of constant l are labelled. The Galactic directions of estimated values of the solar apex (triangles) and antapex (squares) are plotted. The thick dashed line connects the solar motion direction calculated from the Dehnen & Binney (1998) solar space velocities in Table A1. The thin dashed line connects the solar motion direction calculated by Homann (1886), calculated from Seabroke (1879) RVs.

motion, unbiased by the presence of in-falling tidal streams on to the Milky Way disc near the Sun.

This paper has been typeset from a TEX/ LATEX file prepared by the author.

derive the solar motion in the presence of dynamical perturbations altering the kinematics of the solar neighbourhood. They posed the question of whether a subset of stars exists in the solar neighbourhood that has no net radial motion, which can used as a reference against which to measure the solar motion. The simulations of De Simone et al. (2004) demonstrate that transient spiral waves can excite a net radial motion through the solar neighbourhood of $\sim$10 km s^{-1}.

Table A1 also shows that F05 found that the presence of dynamical streams in the solar neighbourhood has a negligible affect on $W^{\odot}_{LSR}$. This suggests that the dynamical streams do not have a net vertical motion because they are well phase-mixed. In this paper, we have shown that there is no net vertical flow through the solar neighbourhood, suggesting $W^{\odot}_{LSR}$ is an appropriate measure of the vertical solar